Available online at www.sciencedirect.com

ScienceDirect

Geochimica et Cosmochimica Acta 132 (2014) 214–237

Geochimica et Cosmochimica Acta

www.elsevier.com/locate/gca

The distribution of geochemical heterogeneities in the source of Hawaiian shield lavas as revealed by a transect across the strike of the Loa and Kea spatial trends: East Molokai to West Molokai to Penguin Bank

Guangping Xu [a,*], Shichun Huang [b], Frederick A. Frey [c,1], Janne Blichert-Toft [d], Wafa Abouchami [e,f], David A. Clague [g], Brian Cousens [h], James G. Moore [i], Melvin H. Beeson [i]

[a] *AIRIE Program, Colorado State University, Fort Collins, CO 80523, United States*
[b] *Harvard University, Cambridge, MA 02138, United States*
[c] *Massachusetts Institute of Technology, Cambridge, MA 02139, United States*
[d] *Laboratoire de Géologie de Lyon, CNRS UMR 5276, Ecole Normale Supériere de Lyon and Université Claude Bernard Lyon I, 46 Allée d'Italie, 69007 Lyon, France*
[e] *Westfälische Wilhelms Universität, Institut für Mineralogie, 48149 Münster, Germany*
[f] *Max Planck Institute for Chemistry, PO box 3060, 55020 Mainz, Germany*
[g] *Monterey Bay Aquarium Research Institute, 7700 Sandholdt Road, Moss Landing, CA 95039, United States*
[h] *Ottawa-Carleton Geoscience Centre, Carleton University, Ontario, Canada*
[i] *U.S. Geological Survey, Menlo Park, CA 94025, United States*

Received 9 April 2013; accepted in revised form 1 February 2014; Available online 12 February 2014

Abstract

An important feature of <2 Ma Hawaiian volcanoes is that they define two sub-parallel spatial trends known as the Loa- and Kea-trends. On the Island of Hawaii, the <1.5 Ma shield lavas on the Loa and Kea spatial trends have distinctive geochemical characteristics that are designated as Loa-type and Kea-type. These geochemical differences are clearly expressed in Sr, Nd, Hf and Pb isotopic ratios, major element contents, and ratios of incompatible elements. They are interpreted to reflect varying proportions of sediment, basalt, gabbro and peridotite in subducted oceanic lithosphere. Pb isotopic ratios indicate that the Loa-type component reflects ancient subduction, >2.5 Ga, whereas the Kea-type component reflects younger subduction, <1.5 Ga. To evaluate the temporal persistence of these geochemical differences in the source of Hawaiian shield lavas, we analyzed lavas from the ~1.5 to 2 Ma Molokai Island volcanoes, East and West Molokai, and the adjacent submarine Penguin Bank. The three volcanoes form a nearly east–west trend that crosscuts the Loa and Kea spatial trends at a high angle; consequently we can determine if these older lavas are Kea-type in the east and Loa-type in the west. All lavas collected from the subaerial flanks of East Molokai, a Kea-trend volcano, have Kea-type geochemical characteristics; however, dive samples collected from Wailau landslide blocks, probably samples of the East Molokai shield that are older than those exposed on the subaerial flanks, include basalt with Loa-type geochemical features. Shield lavas from West Molokai and Penguin Bank, both on the Loa-trend, are dominantly Loa-type, but samples with Kea-type compositions also erupted at

* Corresponding author. Tel.: +1 9706720661.
E-mail addresses: Guangping.Xu@colostate.edu (G. Xu), fafrey@mit.edu (F.A. Frey).
[1] Co-corresponding author.

http://dx.doi.org/10.1016/j.gca.2014.02.002

these Loa-trend volcanoes. The Loa-trend volcanoes, Mahukona, West Molokai, Penguin Bank, and Koolau, have also erupted lavas with Kea-type geochemical characteristics, and the Kea-trend volcanoes, Mauna Kea, Kohala, Haleakala, and East Molokai, have erupted lavas with Loa-type geochemical characteristics. The presence of both Loa- and Kea-type lavas in a volcano provides constraints on the distribution of geochemical heterogeneities in the source of Hawaiian shield basalts. Two plausible models are: (1) source components with Loa- and Kea-type geochemical characteristics are present in the sources of all <2 Ma shields, but the Kea-to-Loa proportion is higher beneath Kea-trend than Loa-trend volcanoes, or (2) the magma source contains a uniform proportion of Loa- and Kea-type components, but these components have different solidi. Magmas derived from the low-temperature regions of the source preferentially sample the component with the lower solidus temperature and form Loa-type lavas. In contrast, magmas derived from the relatively high-temperature regions of the source sample both low and high solidus components in the source and form Kea-type lavas. This model is supported by the linear correlations between isotopic ratios and calculated temperatures of estimated primary magmas.

1. INTRODUCTION

The spatial arrangement of Hawaiian volcanoes from Molokai Island to the Island of Hawaii define two parallel trends known as the Loa- and Kea-trends (Fig. 1a). From the youngest to the oldest, Loa-trend volcanoes are Loihi, Mauna Loa, Hualalai, Mahukona, Kahoolawe, Lanai, and West Molokai, whereas Kea-trend volcanoes are Kilauea, Mauna Kea, Kohala, Haleakala, West Maui, and East Molokai (Fig. 1a). Most of the shield-stage lavas erupted along these two trends have distinctive geochemical characteristics described as Loa- and Kea-type. Specifically, shield lavas from Loa- and Kea-trend volcanoes differ in isotopic ratios of Sr, Nd, Hf, and Pb, incompatible element abundance ratios such as La/Nb and Sr/Nb, and relative abundances of SiO_2 and CaO at a given MgO content. There are, however, complexities, specifically some shields erupted both Loa- and Kea-type lavas, and Loihi lavas, a Loa-trend volcano, have Kea-type SiO_2 and CaO contents (e.g., Fig. 6 of Jackson et al., 2012; Pietruszka et al., 2013). Differences in Pb isotopic ratios between Loa- and Kea type lavas (Tatsumoto, 1978; Abouchami et al., 2005) have been proposed to be the best discriminant of the two types, and have been used to infer the spatial distribution of geochemical heterogeneities in the source of Hawaiian lavas (e.g., Abouchami et al., 2005).

The geochemical differences between Loa- and Kea-trend shield lavas are well established for the volcanoes forming the Island of Hawaii. East Molokai, West Molokai, and Penguin Bank volcanoes constructed at ~1.5 to 2 Ma form a nearly east to west trend that crosses the Loa- and Kea-spatial trends at a high angle (Fig. 1a). Consequently, lavas from these Molokai Island volcanoes can be used to evaluate if the geochemical differences between <1 Ma Loa- and Kea-trend volcanoes forming the Island of Hawaii were already present at ~1.5 to 2 Ma. Previously we showed that: (1) Lavas on the subaerial flanks of the Kea-trend East Molokai volcano (~1.5 Ma) are Kea-type in their geochemical characteristics, whereas lavas collected from submarine Wailua landslide blocks, likely to be older East Molokai shield lavas, include basalt with Loa-type geochemical characteristics (Xu et al., 2005); (2) Lavas from West Molokai volcano (~1.8 Ma) on the Loa-trend range from Loa-type to Kea-type in their geochemistry (Xu et al., 2007). In this paper we present and interpret compositional and isotopic data for lavas from Penguin Bank, a previously unstudied volcano west of West Molokai volcano (Fig. 1).

2. GEOLOGICAL SETTING

Penguin Bank, West and East Molokai, Lanai, West and East Maui, and Kahoolawe are the seven volcanoes that constituted the island of Maui Nui (e.g., Price and Elliott-Fisk, 2004). West Molokai has two rift zones defined by postshield cones and ridges that extend northwest and southwest from the summit (Fig. 1b). The southwest rift zone is aligned with Penguin Bank, leading to the idea that Penguin Bank might be a long submarine rift zone of West Molokai (Stearns, 1946). It was later proposed to be a separate Hawaiian volcano (Macdonald, 1972; Clague and Sherrod, in press), an interpretation supported by recent bathymetric data collected on the shallow carbonate platform that show a western shoal separated from the slope of West Molokai by a saddle at a depth of ~55 m (Eakins et al., 2003) (Fig. 1c). The spatial configuration of Penguin Bank, West Molokai, and East Molokai, nearly perpendicular to the main trend of the Hawaiian chain (Fig. 1a), provides the opportunity to evaluate the longevity and to understand the origin of geochemical differences between lavas erupted along the Loa- and Kea-trends.

3. OBJECTIVES

We use major and trace element compositions and Sr, Nd, Hf and Pb isotopic ratios of Penguin Bank lavas to address several questions and posits: (a) Are there geochemical similarities between Penguin Bank and West Molokai lavas that support the interpretation that Penguin Bank is a submarine rift zone of West Molokai? (b) Does the trend from East Molokai, a Kea-trend volcano with dominantly Kea-type geochemical characteristics, to West Molokai, a Loa-trend volcano with lavas having both Loa- and Kea-type geochemical characteristics, persist to Penguin Bank? Specifically, is Penguin Bank a Loa-trend volcano with only Loa-type geochemical characteristics? (c) How many isotopically distinct components contributed to Penguin Bank lavas? (d) Geochemical data for Penguin

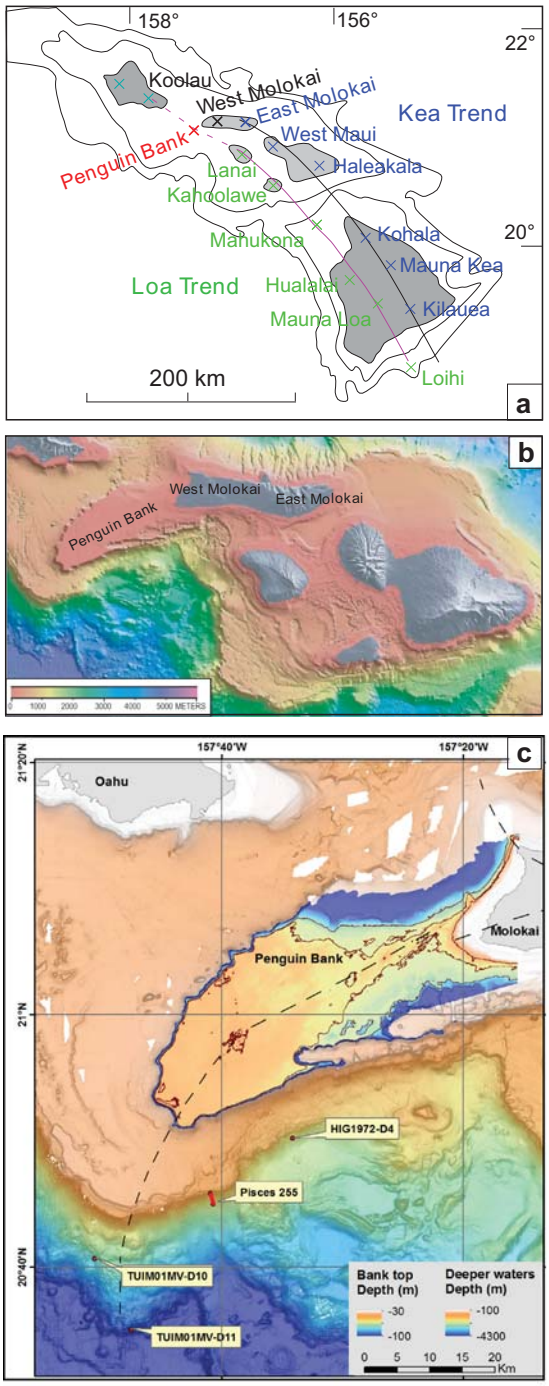

Fig. 1. (a) Young, <2 Ma, Hawaiian volcanoes showing the spatially defined Loa and Kea trends. West Molokai and Penguin Bank are the oldest volcanoes on the Loa-trend. East Molokai is the oldest volcano on the Kea-trend. (b) Map of the volcanoes comprising the former large island of Maui Nui (modified from Eakins et al., 2003). East Molokai, West Molokai, and Penguin Bank define a transect, nearly perpendicular to the strike of the Loa and Kea trends. (c) Bathymetry of Penguin Bank indicated by 30–100 m depth contours (Bank top depth in legend). Penguin Bank is defined by the blue 100 m contour line surrounding "Penguin Bank" on the map and it shoals to 30 m (see legend labeled "Bank top Depth"). Deep waters in the region are defined by the 100 and 4300 m contours surrounding Penguin Bank (see legend labeled "Deeper waters Depth"). Dashed lines are rift zones of West Molokai and Penguin Bank. The sampling locations are shown as: HIG 1972-D4 (2 dredge samples); Pisces 255 (13 samples collected on *Pisces V* dive designated as P5-255-1 to -16); TUIMO 1MV-D10 (5 dredge samples collected by the RV Melville) and TUIMO 1MV-D11 (12 glass sand grains separated from a volcaniclastic rock collected by the RV Melville). (For interpretation of the references to color in this figure legend, the reader is referred to the web version of this article.)

Bank lavas will determine whether the geochemical differences between Loa- and Kea-trend volcanoes ceased at Lanai (Loa-trend) and Haleakala (Kea-trend) (Fig. 1a) as proposed by Abouchami et al. (2005). (e) Isotopic data for Penguin Bank lavas will constrain the spatial distribution of the high-$^{87}Sr/^{86}Sr$ and low-$^{143}Nd/^{144}Nd$ component found in shields formed near the Molokai Fracture Zone (Basu and Faggart, 1996). Specifically, do Penguin Bank lavas contain the extremely enriched (i.e., high $^{87}Sr/^{86}Sr$ up to 0.7046 and correspondingly low $^{143}Nd/^{144}Nd$) component that is expressed in Loa-trend lavas erupted northwest (Koolau) and southeast (Lanai and Kahoolawe) of Penguin Bank (Fig. 1a), and also in a submarine basalt collected ~20 km from the north coast of West Molokai (Xu et al., 2007)? (f) What is the spatial distribution of magma sources with Loa- and Kea-type geochemical characteristics in the Hawaiian plume?

4. SAMPLES

Fourteen volcanic whole-rock samples were collected on the southern flank of Penguin Bank during a single *Pisces V* submersible dive from water depths of 1815 m for P5-255-1 to 1210 m for P5-255-16 (Table S1; Fig. 1c). Also, numerous scoop samples of sediments (mostly gravels and pebbles) collected during this dive contained basaltic glass (Table S2). Two HIG1972-D4 basalt samples were dredged from the southern margin of Penguin Bank, northeast of the Pisces dive location (Fig. 1c). Five basalt samples from the southwestern extremity of Penguin Bank (Fig. 1b) were selected from material recovered by dredge 10 of the 2005 TUIM01 cruise of the R/V Melville; these samples are designated MV-D10. Twelve glass sand grains separated from a volcaniclastic rock collected by dredge 11 of the 2005 TUIM01 cruise of the R/V Melville are designated MV-D11.

5. ANALYTICAL TECHNIQUES

Olivine crystals were analyzed on a Cameca SX-100 5-spectrometer electron microprobe at University of California at Davis using natural (Aoli olivine 174.1 for Si and Mg, rhodonite for Mn, chromite for Cr, augite for Ca) and synthetic (Ni-olivine for Ni, fayalite for Fe) standards (Table S2). Standards analyzed as unknowns are within 1% of stoichiometric balance.

Major element compositions of glass occurring as sand grains, rinds on basalt, in gravel clasts, and as inclusions in olivine were analyzed by electron microprobe at the U.S. Geological Survey in Menlo Park (Table S2) using natural and synthetic standards as described in Davis et al. (1994) with MgO adjusted to 7.07 wt% for Smithsonian glass standard VG2.

Prior to whole-rock analyses, sawed rock slabs were immersed in distilled water for one week and then were broken into chips that were washed in an ultrasonic bath three times (5 min each) using MQ-H_2O, and dried on a hotplate before crushing into fine powder in an agate shatterbox. Major element contents for whole-rock samples (Table 1) were determined by X-ray fluorescence (XRF) at the Geoanalytical Laboratory at Washington State University for the MV-D10 samples, at the University of Massachusetts, Amherst, for the P5-255 samples, and at the U.S. Geological Survey (USGS) laboratory for the two HIG1972-D4 samples.

Table 1
Major element compositions of Penguin Bank whole-rock samples.

Sample	LAB	SiO_2	TiO_2	Al_2O_3	Fe_2O_3	FeO	MnO	MgO	CaO	Na_2O	K_2O	P_2O_5	Total
Melville dredge													
MV-D10-R1	WSU	50.29	2.23	12.59		11.01	0.17	10.91	9.90	2.16	0.48	0.25	100.0
MV-D10-R2	WSU	50.37	2.23	12.54		10.96	0.17	11.03	9.88	2.13	0.44	0.25	100.0
MV-D10-R4	WSU	50.41	2.26	12.69		11.08	0.17	10.57	9.98	2.15	0.44	0.25	100.0
MV-D10-R5	WSU	51.20	2.47	13.61		10.91	0.17	7.71	10.71	2.42	0.51	0.28	100.0
MV-D10-R6	WSU	50.78	2.29	12.87		10.67	0.17	10.18	10.11	2.22	0.45	0.26	100.0
Pisces V dive													
P5-255-1	UMASS	49.45	2.21	12.13	12.52		0.17	11.41	9.24	2.02	0.44	0.28	99.9
P5-255-2	UMASS	49.83	2.3	12.65	12.18		0.17	9.71	9.97	2.11	0.48	0.31	99.7
P5-255-3	UMASS	49.64	2.2	12.11	12.61		0.17	11.21	9.15	2.09	0.46	0.27	99.9
P5-255-5	UMASS	50.81	2.45	13.66	12.38		0.18	6.78	10.51	2.35	0.52	0.3	99.9
P5-255-6	UMASS	50.71	2.44	13.61	12.39		0.18	6.82	10.57	2.31	0.5	0.31	99.8
P5-255-7	UMASS	48.02	1.95	10.71	12.51		0.17	15.85	7.98	1.74	0.4	0.24	99.6
P5-255-8	UMASS	48.08	1.95	10.8	12.5		0.17	15.77	8.14	1.89	0.38	0.25	99.9
P5-255-9	UMASS	47.43	2.04	11.02	12.9		0.17	15.4	8.41	1.98	0.41	0.26	100.0
P5-255-10	UMASS	47.77	2.07	11.08	12.77		0.17	14.89	8.42	2.12	0.43	0.26	100.0
P5-255-11	UMASS	47.81	2.14	11.31	12.79		0.18	13.99	8.74	2.25	0.43	0.29	99.9
P5-255-14	UMASS	49.8	2.36	12.85	12.45		0.17	9.89	9.74	1.99	0.47	0.29	100.0
P5-255-15	UMASS	50.52	2.46	13.76	12.45		0.18	6.74	10.61	2.81	0.49	0.3	100.3
P5-255-16	UMASS	49.02	2.14	11.82	12.59		0.17	12.37	8.98	1.94	0.43	0.26	99.7
HIG dredge													
HIG1972-D4-1	USGS	49.90	1.88	12.4		11.15	0.17	12.1	9.93	2.09	0.26	0.19	100.1
HIG1972-D4-2	USGS	49.69	1.90	12.67		11.05	0.17	11.47	10.46	2.08	0.26	0.25	100.0

The contents are wt %. All iron reported as FeO for analyses at Washington State University (WSU) and the United States Geological Survey (USGS) and as Fe_2O_3 at the University of Massachusetts (UMASS). Analyses done at WSU are normalized to 100%.

Table 2
Trace element compositions of Penguin Bank whole-rock samples.

Sample	La	Ce	Pr	Nd	Sm	Eu	Gd	Tb	Dy	Ho	Er	Tm	Yb	Lu	Ba	Th	Nb	Y	Hf	U	Pb	Rb	Cs	Sr	Sc	Zr
Melville dredge																										
MV-D10-R1	9.06	23.7	3.66	17.7	4.88	1.68	5.27	0.85	4.78	0.94	2.42	0.34	1.91	0.28	68.4	0.61	9.29	25.6	3.46	0.20	0.85	6.3	0.09	299	26.6	129
MV-D10-R2	9.03	24.1	3.65	17.7	4.77	1.63	5.26	0.85	4.69	0.93	2.35	0.35	1.91	0.28	69.7	0.60	9.37	25.5	3.45	0.21	0.83	5.7	0.07	298	27.2	129
MV-D10-R4	9.34	25.0	3.75	17.9	4.82	1.67	5.30	0.86	4.78	0.94	2.37	0.35	1.94	0.28	71.6	0.61	9.64	26.5	3.45	0.20	0.80	5.9	0.07	312	27.9	134
MV-D10-R5	10.3	27.4	4.13	19.8	5.32	1.83	5.83	0.94	5.21	1.01	2.58	0.37	2.11	0.30	78.6	0.67	10.5	29.0	3.77	0.23	0.91	6.6	0.09	336	30.5	147
MV-D10-R6	9.48	24.5	3.75	17.9	4.95	1.70	5.36	0.86	4.80	0.95	2.44	0.35	1.95	0.28	71.6	0.63	9.66	27.1	3.57	0.21	0.87	5.9	0.07	316	28.2	135
Pisces V dive																										
P5-255-1	10.1	26.3	3.99	19.3	5.13	1.75	5.46	0.86	4.75	0.93	2.40	0.34	1.91	0.27	76.6	0.67	10.3	26.0	3.70	0.24	1.11	5.62	0.07	326	26.3	143
P5-255-2	10.8	27.9	4.26	20.4	5.48	1.83	5.79	0.91	5.06	0.98	2.49	0.36	1.96	0.29	78.5	0.73	10.9	27.7	3.91	0.34	0.98	6.12	0.08	354	28.9	154
P5-255-3	9.90	26.3	4.02	19.1	5.13	1.72	5.41	0.86	4.75	0.91	2.32	0.34	1.89	0.27	75.9	0.68	10.3	25.5	3.71	0.22	0.93	6.09	0.08	322	26.2	142
P5-255-5	11.0	28.9	4.33	21.0	5.69	1.92	6.04	0.96	5.34	1.02	2.60	0.39	2.12	0.30	80.5	0.74	11.2	29.5	3.95	0.25	0.99	6.98	0.11	366	30.4	155
P5-255-6	11.0	29.1	4.30	20.5	5.53	1.88	5.96	0.95	5.33	1.02	2.62	0.38	2.10	0.30	79.1	0.78	11.1	29.3	3.92	0.24	1.00	6.52	0.09	363	30.8	154
P5-255-7	8.62	22.8	3.55	17.1	4.66	1.59	4.98	0.80	4.41	0.84	2.19	0.31	1.73	0.25	68.0	0.63	9.34	22.8	3.38	0.21	0.81	5.22	0.06	280	22.6	129
P5-255-8	8.56	22.1	3.57	16.8	4.73	1.57	4.95	0.79	4.40	0.84	2.21	0.32	1.76	0.25	61.4	0.61	8.76	22.9	3.34	0.20	0.77	4.69	0.06	276	21.7	122
P5-255-9	10.0	26.0	3.94	18.6	5.01	1.68	5.26	0.83	4.66	0.89	2.29	0.33	1.81	0.26	70.6	0.77	10.9	23.8	3.66	0.25	0.82	5.24	0.06	297	23.1	135
P5-255-10	10.6	26.4	4.09	19.0	5.14	1.72	5.40	0.85	4.72	0.90	2.30	0.33	1.80	0.26	78.8	0.80	11.2	24.9	3.65	0.27	0.86	5.96	0.07	304	23.8	139
P5-255-11	10.9	27.9	4.16	19.5	5.30	1.75	5.56	0.88	4.86	0.94	2.35	0.34	1.87	0.27	80.3	0.81	11.6	25.4	3.80	0.27	0.87	5.64	0.07	319	24.0	142
P5-255-14	9.91	25.8	3.94	19.1	5.22	1.78	5.56	0.88	4.96	0.95	2.42	0.35	1.96	0.28	74.8	0.70	10.6	26.7	3.68	0.26	0.85	5.91	0.07	323	28.6	145
P5-255-15	10.8	28.1	4.27	20.6	5.57	1.88	5.99	0.97	5.35	1.03	2.66	0.39	2.13	0.30	77.0	0.77	10.8	27.6	3.98	0.25	0.99	5.79	0.07	340	28.5	148
P5-255-16	9.95	25.8	3.99	19.1	5.18	1.74	5.45	0.87	4.89	0.93	2.34	0.34	1.93	0.28	71.8	0.67	10.4	26.0	3.72	0.22	0.94	5.51	0.07	319	27.7	142
HIG dredge																										
HIG1972-D4-1	6.10	16.0	2.63	13.1	3.89	1.38	4.47	0.74	4.13	0.81	2.12	0.31	1.77	0.25	49.0	0.41	6.83	22.2	2.78	0.14	0.59	3.54	0.04	228	27.2	98.0
HIG1972-D4-2	6.26	16.1	2.66	13.2	3.98	1.39	4.50	0.74	4.26	0.83	2.15	0.32	1.81	0.27	50.8	0.43	6.96	22.7	2.77	0.17	0.70	3.56	0.05	244	27.0	98.5
Standard																										
BHVO-2	15.2	38.1	5.53	24.9	6.15	2.04	6.12	0.96	5.27	1.00	2.49	0.36	2.04	0.28	135.5	1.31	18.9	28.1	4.41	0.44	1.58	9.39		395	31.9	176
1σ ($n = 7$)	0.4	0.8	0.12	0.5	0.14	0.05	0.13	0.02	0.12	0.02	0.06	0.02	0.06	0.01	3.6	0.03	0.5	0.6	0.11	0.01	0.06	0.23		11	0.7	5

Table 3
Sr, Nd, Hf and Pb isotope data for Penguin Bank whole-rock samples.

Sample name	$^{87}Sr/^{88}Sr$	2σ	$^{176}Hf/^{177}Hf$	2σ	$^{143}Nd/^{144}Nd$	2σ	$^{206}Pb/^{204}Pb$	2σ	$^{207}Pb/^{204}Pb$	2σ	$^{208}Pb/^{204}Pb$	2σ
MV-D10-R2	0.703773	0.000007	0.283088	0.000003	0.512945	0.000005	18.1011	0.0027	15.4597	0.0034	37.8510	0.0110
MV-D10-R4	0.703768	0.000005	0.283092	0.000004	0.512935	0.000005	18.0987	0.0026	15.4572	0.0033	37.8450	0.0105
MV-D10-R4 dup							18.0985	0.0014	15.4570	0.0018	37.8445	0.0056
MV-D10-R5	0.703760	0.000004	0.283091	0.000004	0.512953	0.000005	18.1020	0.0029	15.4603	0.0036	37.8523	0.0117
MV-D10-R5 dup							18.1018	0.0017	15.4600	0.0020	37.8514	0.0065
P5-255-2			0.283092	0.000004	0.512948	0.000005	18.1598	0.0040	15.4686	0.0052	37.8550	0.0165
P5-255-6			0.283093	0.000004	0.512942	0.000004	18.1016	0.0036	15.4611	0.0045	37.8394	0.0145
P5-255-7	0.703759	0.000010	0.283097	0.000004	0.512955	0.000005	18.1561	0.0017	15.4638	0.0021	37.8576	0.0068
P5-255-8	0.703753	0.000010	0.283096	0.000004	0.512952	0.000005	18.1562	0.0021	15.4643	0.0027	37.8592	0.0089
P5-255-9	0.703648	0.000010	0.283105	0.000004	0.512967	0.000004	18.2917	0.0028	15.4721	0.0035	37.9505	0.0114
P5-255-10	0.703650	0.000011	0.283110	0.000003	0.512969	0.000005	18.2975	0.0030	15.4756	0.0036	37.9620	0.0118
P5-255-11	0.703651	0.000008	0.283109	0.000004	0.512966	0.000005	18.2946	0.0026	15.4728	0.0032	37.9523	0.0104
P5-255-15			0.283096	0.000003	0.512949	0.000003	18.1016	0.0033	15.4606	0.0041	37.8371	0.0135
P5-255-15 dup							18.1025	0.0022	15.4617	0.0028	37.8407	0.0092
HIG1972-D4-1	0.703883	0.000011	0.283073	0.000004	0.512912	0.000004	18.1360	0.0025	15.4475	0.0032	37.9311	0.0104
HIG1972-D4-2	0.703854	0.000010	0.283073	0.000003	0.512907	0.000004	18.1298	0.0016	15.4462	0.0020	37.9228	0.0064

Samples with postfix "dup" are duplicate run on TIMS with separate filament loading.
$^{87}Sr/^{88}Sr$ for Melville dredged samples (i.e., MV-D10-R2, MV-D10-R4 and MV-D10-R5) were analyzed at Carleton University following the procedures of Cousens et al. (2003) and the rest were analyzed at MIT following the procedure of Xu et al. (2007).

Trace element abundances were determined at MIT by inductively-coupled plasma mass spectrometry (ICP-MS) (Table 2) using a Fisons VG Plasmaquad 2 + S with both internal and external drift monitors. Trace element results are reported as the mean of duplicate analyses obtained on different days. The analytical procedures and estimates of accuracy and precision were discussed by Huang and Frey (2003). The mean and standard deviation (1σ) for BHVO-2 is listed in Table 2.

A subset of 13 Penguin Bank lavas were selected for measurement of Sr, Nd, Hf and Pb isotopic ratios (Table 3). Strontium isotopic ratios were determined on acid-leached residues by thermal ionization mass spectrometry (TIMS) at MIT and Carleton University following the acid leaching and analytical procedures of Xu et al. (2007) and Cousens et al. (2003), respectively (Table 3). Instrumental mass fractionations were normalized to $^{86}Sr/^{88}Sr = 0.1194$ using the exponential law. Mean measured $^{87}Sr/^{86}Sr$ for NIST SRM987 during the course of study at MIT was 0.710240 ± 0.000013 (2σ, $n = 27$) and at Carleton University was 0.710244 ± 0.000015 (2σ, $n = 20$).

Neodymium and Hf were separated from the same acid dissolutions of 13 Penguin Bank samples at the Ecole Normale Supérieure (ENS) in Lyon, and their isotopic ratios were measured using a Nu Plasma 500 HR MC-ICP-MS (multiple-collector inductively-coupled plasma mass spectrometer) coupled with a desolvating nebulizer Nu DSN-100, also at ENS-Lyon (Table 3). The chemical separation procedures and mass spectrometric protocols followed those described in Blichert-Toft et al. (1997) and Blichert-Toft and Albarède (2009). Instrumental mass fractionation for Nd and Hf was corrected to, respectively, $^{146}Nd/^{144}Nd = 0.7219$ and $^{179}Hf/^{177}Hf = 0.7325$, using an exponential law. External analytical reproducibility and accuracy of both $^{143}Nd/^{144}Nd$ and $^{176}Hf/^{177}Hf$ were estimated from repeated runs of the Lyon JMC in-house Nd standard and the JMC-475 Hf standard. Specifically, eight measurements of the Lyon JMC in-house Nd standard gave $^{143}Nd/^{144}Nd$ of 0.512131 ± 0.000005 (2σ), corresponding to a value of 0.511946 for the "Rennes" in-house Nd standard and 0.511841 for the La Jolla Nd standard (Chauvel and Blichert-Toft, 2001). The $^{143}Nd/^{144}Nd$ ratios reported in Table 3 have been normalized to $^{143}Nd/^{144}Nd_{La\ Jolla} = 0.511856$. Six measurements of the JMC-475 Hf standard gave $^{176}Hf/^{177}Hf$ of 0.282165 ± 0.000003 (2σ). Since this is identical within error to the accepted value of 0.282163 ± 0.000009 (Blichert-Toft et al., 1997), no corrections were applied to the $^{176}Hf/^{177}Hf$ data reported in Table 3. In-run analytical errors for all samples for both elements were similar to the external errors quoted here for the repeated standard analyses. Both Nd and Hf total procedural blanks were <20 pg.

Lead isotopic ratios were determined on acid-leached residues prepared at the Max Planck Institute for Chemistry (Mainz) on a ThermoFisher Triton TIMS instrument using the triple spike technique (Galer, 1999). Coarse-crushed powders (0.1–0.2 g) were used for Pb isotopic analysis and chemical procedures are similar to those described in Abouchami et al. (2000). In the two analytical sessions devoted to analyses of Penguin Bank samples, average results of the NIST SRM981 standard were $^{206}Pb/^{204}Pb = 16.9428 \pm 0.0012$, $^{207}Pb/^{204}Pb = 15.5004 \pm 0.0006$ and $^{208}Pb/^{204}Pb = 36.7313 \pm 0.0026$ (2σ, $n = 4$) and agree within error with the values reported by Galer and Abouchami (1998). The procedural Pb blank analyzed in parallel with the samples was 26 pg.

6. RESULTS

6.1. Petrography

The P5-255 samples include picritic lavas with large (several mm) spinel-bearing olivine crystals and smaller

plagioclase and clinopyroxene crystals; a second group has fewer large olivine crystals, and clinopyroxene and plagioclase crystals of similar size; a third group has rare olivine phenocrysts, and microphenocrysts of plagioclase and clinopyroxene. Glasses in all the samples contain abundant microlites of clinopyroxene and plagioclase. Most samples are dense, and presumably quenched after subaerially degassed flows entered the ocean where increasing water pressure caused re-solution of the volatiles in the bubbles (Moore and Clague, 1987). A few clasts in scoop samples and breccia clasts collected at the shallowest depths are highly vesicular (Table S1). These breccias are carbonate-cemented, commonly with vesicular glassy olivine-rich fragments set in a shallow water carbonate matrix that includes algal fragments, large reef foraminifera, gastropods, clamshells, and bryozoans. The olivine phenocrysts include euhedral, deformed, skeletal, and resorbed and rounded crystals, as typically seen in Hawaiian tholeiitic picrites. Sample P5-255-14 contains a cm-sized open-textured xenolith of plagioclase, clinopyroxene and glass, and sample P5-255-13 contains an olivine rimmed by orthopyroxene, in turn rimmed by clinopyroxene. Plagioclase microphenocrysts commonly enclose clinopyroxene, indicating clinopyroxene on the liquidus prior to plagioclase.

Melville DR-11 recovered a volcaniclastic rock containing sand-sized chips of glass. Melville DR-10 recovered whole-rocks ranging from highly to slightly vesicular and from olivine-phyric to rarer clinopyroxene-phyric to clinopyroxene- and plagioclase-phyric. The glasses have abundant microlites. The two HIG1972-D4 samples are nearly identical and contain abundant euhedral olivine microphenocrysts with smaller plagioclase and clinopyroxene crystals set in a slightly to moderately (3–10%) vesicular groundmass.

6.2. Major element compositions

6.2.1. Olivines

The 111 analyses of olivine phenocryst cores in 8 samples (Table S2) range in composition from forsterite (Fo) 77.8–89.0%, NiO 0.25–0.47%, CaO 0.18–0.31% and MnO 0.13–0.26%. The abundance of NiO correlates positively with Fo content (Fig. 2). MnO and CaO abundances (not shown) correlate inversely with Fo content.

6.2.2. Glasses

Compositions of unaltered glasses are important because they represent melt compositions. A plot of total alkali ($Na_2O + K_2O$ content) vs. SiO_2 content is commonly used to classify Hawaiian lavas (e.g., Macdonald and Katsura, 1964). All Penguin Bank glasses, i.e., occurring as sand grains, clasts, as rinds on pillow basalts, and as inclusions in olivine, have >50% SiO_2 and they range from tholeiitic basalt to basaltic andesite (Fig. 3). Most of the glass inclusions have relatively high SiO_2 contents (52–55%), with a substantial range in total alkali content (2.7–3.7%). Many of the glasses from pillow rinds and clasts overlap with the glass inclusions (Fig. 3). However, a group of glasses from pillow rinds and clasts form a distinct field with low SiO_2 contents of ~51% and total alkali contents of 2.7–3.5% (circled in Fig. 3).

Glasses occurring as sand grains in a Melville Dr 11 volcanoclastic rock range in MgO from 7% to 10% and fill the compositional gap between the whole-rocks (>9% MgO) and the low-MgO (4.5–6.6%) glasses from Penguin Bank (Fig. 4). Similar trends are defined by whole-rock shield lavas with <7.5% MgO from West and East Molokai (Fig. 4). The peak in CaO content at 7% MgO in Penguin Bank lavas reflects the importance of olivine fractionation followed by clinopyroxene fractionation as MgO decreases to <7% in Hawaiian shield lavas (e.g., Wright and Fiske, 1971).

6.2.3. Whole-rocks

Post-magmatic processes may affect the composition of submarine lavas. K_2O/P_2O_5, a ratio sensitive to alteration processes (e.g., Feigenson et al., 1983; Frey et al., 1990, 1994; Jackson et al., 1999), in Penguin Bank whole-rocks falls within the range (1.5–2) of recently erupted, unaltered shield lavas from Kilauea volcano (Garcia et al., 2000) and historical Mauna Loa lavas (Rhodes, 1995) (Fig. S1).

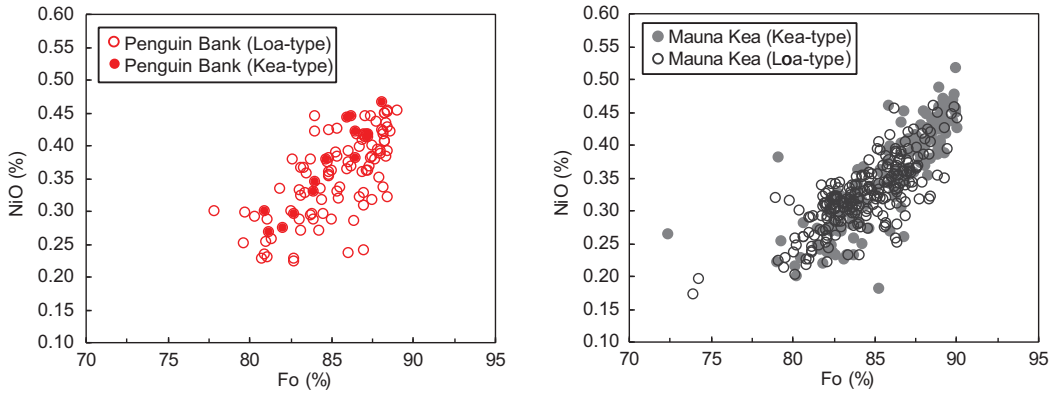

Fig. 2. NiO abundance vs. forsterite (Fo) content of olivine phenocrysts in Loa- and Kea-type (as defined by Pb isotopic ratios, Abouchami et al., 2005) shield lavas from (a) Penguin Bank and (b) Mauna Kea. At both volcanoes the NiO and Fo contents of olivine phenocrysts are positively correlated, but the fields for Loa- and Kea-type lavas overlap. Data for Mauna Kea from Putirka et al. (2011). Note that these authors mistakenly labeled the uppermost lavas in the Hawaii Scientific Drill Core (samples R8 to R120 in their Tables A1a, A2a) as Mauna Kea lavas but they are from Mauna Loa (Rhodes and Vollinger, 2004); consequently they are not plotted in this figure.

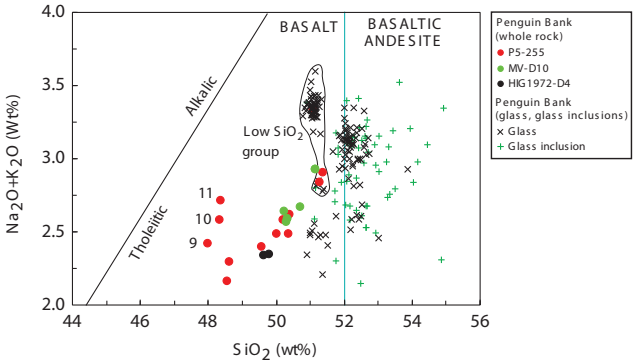

Fig. 3. $Na_2O + K_2O$ vs. SiO_2 content for Penguin Bank whole-rocks, associated glasses, glass sand grains in a volcaniclastic rock and glass inclusions in olivine. Whole-rocks and associated glasses are tholeiitic basalt and glass inclusions in olivine phenocrysts are dominantly basaltic andesite. Whole-rocks P5-255-9, -10, and -11 with the lowest SiO_2 contents are labeled. Note the cluster of glasses with 51% SiO_2 and total alkalis from 2.7% to 3.7%. The circled glasses are the low-SiO_2 group in Fig. 4a. The alkalic-tholeiitic dividing line is from Macdonald and Katsura (1964). The measured whole-rock compositions were adjusted assuming that the measured iron content, as Fe_2O_3, should be divided into Fe_2O_3 and FeO assuming a molar ratio of 0.1 for $Fe^{3+}/(Fe^{2+} + Fe^3)$. In the glasses, all the Fe is assumed to be FeO.

Whole-rock sample HIG1972-D4-2 has the lowest K_2O/P_2O_5 (~1). The whole-rock Ba/Rb ratio, another ratio sensitive to alteration, ranges from 11.5 to 14.3, similar to the average of 12.4 for oceanic island basalt (OIB) (Hofmann and White, 1983). Again the outlier is sample HIG1972-D4-2, which has anomalously low K_2O/P_2O_5 and high Ba/Rb (Fig. S1). The inverse trend defined by Penguin Bank whole-rock samples in K_2O/P_2O_5 vs. Ba/Rb may indicate loss of K and Rb; consequently, these elements are not considered in the subsequent discussion.

All whole-rocks recovered from Penguin Bank are tholeiitic basalt although relative to other lavas from Penguin Bank, samples P5-255-9, -10, and -11 are offset toward the alkalic field because of their low SiO_2 contents of 47.4–47.8% (Fig. 3). SiO_2 content in Penguin Bank lavas increases with decreasing MgO content reflecting fractionation of the SiO_2-poor mineral olivine (Fig. 4a).

The two HIG1972-D4 Penguin Bank samples, however, have higher CaO contents at a given MgO content than other Penguin Bank samples (Fig. 4b). In contrast to the scatter in CaO content at a given MgO content, Al_2O_3 vs. MgO for Penguin Bank, West Molokai, and East Molokai lavas with >7 wt% MgO forms a well-defined trend consistent with addition of Fo_{85} olivine (Fig. 4c).

As typical of Hawaiian shield lavas, total iron as Fe_2O_3 does not vary systematically at >7% MgO content (Fig. 4d) (Clague et al., 1995; Rhodes and Vollinger, 2004). TiO_2 content is not a discriminant between lavas from the three Molokai shields. However, the two HIG1972-D4 samples from Penguin Bank that have relatively high CaO contents are clearly offset to lower TiO_2 contents (Fig. 4e). Also, the Pisces samples P5-255-9, -10, and -11, which have relatively low SiO_2 contents, have slightly higher TiO_2 concentrations at a given MgO (Fig. 4e).

6.3. Incompatible trace element abundances in whole rocks

An overview of incompatible trace element abundances in Penguin Bank samples is provided by a primitive mantle (PM) normalized plot (Fig. 5). Like most Hawaiian shield lavas, Penguin Bank lavas are relatively enriched in light REE with average $(La/Yb)_{PM} = 3.71 \pm 0.22$ (1σ, $n = 13$), $(La/Sm)_{PM} = 1.25 \pm 0.22$, and $(La/Ce)_{PM} = 0.99 \pm 0.02$. Furthermore, Fig. 5 shows that basalts from Penguin Bank are enriched in Sr ($(Sr/Nd)_{PM} = 1.09 \pm 0.04$, 1σ), and relatively depleted in Th. Unusually high Ba/Th, typically greater than 100, is characteristic of Hawaiian basalts and significantly higher than Ba/Th of PM, MORB, and most OIB (e.g., Yang et al., 2003). Hofmann and Jochum (1996) suggested that anomalously high Ba/Th in Hawaiian basalts reflects a recycled component in their source, such as plagioclase-rich gabbro formed in the lower oceanic crust. This inference is consistent with whole-rock $(Sr/Nd)_{PM} > 1$ and the extreme Sr enrichment in rare melt inclusions in olivines from Mauna Loa Volcano (Sobolev et al., 2000). However, Sr/Nd and Ba/Th do not distinguish Loa- and Kea-trend lavas (Hofmann and Jochum, 1996; Huang and Frey, 2003). A complexity is that Ba mobility during post-magmatic alteration (Huang and Frey, 2003) may have destroyed a significant correlation between Sr/Nd and Ba/Th (e.g., Fig. 10 of Yang et al., 2003; Pietruszka et al., 2013).

The two HIG1972-D4 dredge lavas are geochemically distinct from the other Penguin Bank lavas and most basalts forming other Hawaiian shields; i.e., the HIG samples have nearly flat trends from La to Eu (Fig. 5), low TiO_2 contents (Fig. 4e), low abundances of highly incompatible trace elements, e.g., Th (Fig. 6a). In contrast, samples P5-255-9, -10 and -11, with the highest alkalinity, i.e. closest to the alkalic field in Fig. 3, and with relatively high MgO contents (Fig. 4a), have relatively high abundances of highly incompatible trace elements, such as Th (Fig. 6a). (Xu et al., 2005, 2007). Except for sample P5-255-2, the U content of Penguin Bank lavas is correlated with Th abundance (Fig. 6a), thereby showing that U was not significantly mobilized by alteration. Ratios of Th/U are similar in Penguin Bank samples, 2.95 ± 0.22 (1σ, $n = 23$), and the Kea-trend Mauna Kea basalts, 2.97 ± 0.38

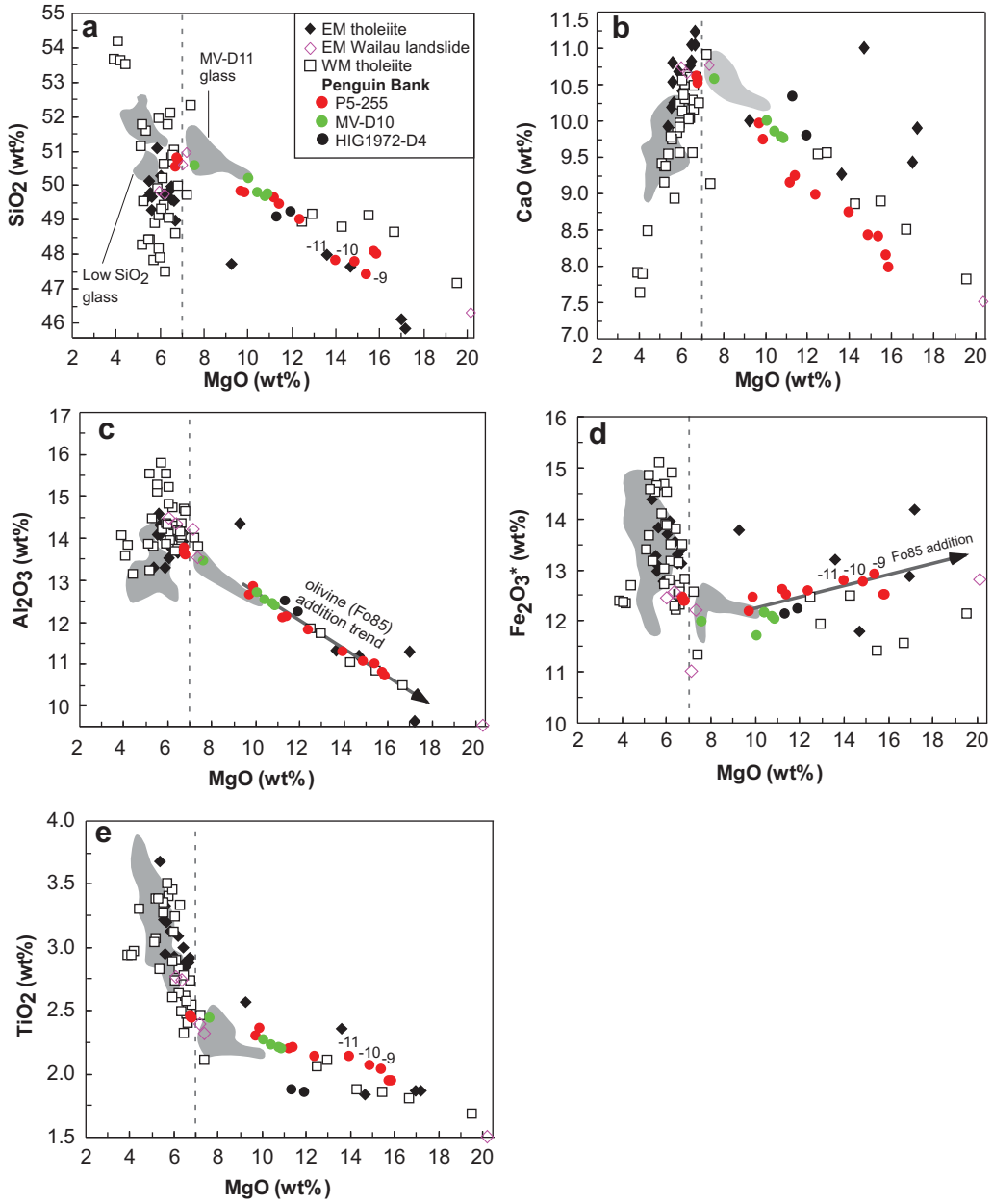

Fig. 4. SiO_2, CaO, Al_2O_3, Fe_2O_3 (as total iron) and TiO_2 vs. MgO content. Samples P5-255-9, -10, and -11 with slightly high Fe_2O_3 and TiO_2 and lower SiO_2 are labeled as "-9, -10, and -11". Penguin Bank glasses are shown as the gray fields; note the bimodality in SiO_2 content at <7% MgO; the field of low-SiO_2 group glasses is labeled. Also labeled is a field for glasses with >7% MgO; these samples are from a volcaniclastic rock recovered by MV-D11. East Molokai data are from Xu et al. (2005) and Tanaka et al. (2002) and West Molokai data are from Xu et al. (2007). Panels c and d show trends for addition of Fo_{85} olivine.

(1σ, $n = 144$; from Huang and Frey, 2003), and are within the ranges reported for Mauna Loa (2.92 ± 0.02) and Kilauea (3.01 ± 0.01) by Jochum and Hofmann (1995).

Many incompatible element abundance ratios are similar in Loa- and Kea-trend lavas, and these ratios are typical of ocean island basalt (OIB). For example, $(Zr/Sm)_{PM}$ and $(Zr/Hf)_{PM}$ ratios range from 1.0 to 1.3 (Fig. 6b and David et al., 2000). These ratios are not correlated with radiogenic isotope ratios and do not distinguish Loa- and Kea-type lavas. Ce/Pb ranges from 22.9 to 32.1 in Penguin Bank samples, similar to the average ratios of 33.6 and 29.7 of East and West Molokai lavas, respectively (Xu et al., 2005, 2007), and consistent with the average OIB value of 25 ± 5 (Hofmann et al., 1986). Nb/U in Penguin Bank samples ranges from 41.5 to 50.6 with an average of 44.8 ± 2.0 (1σ, $n = 15$), which is similar to that in Mauna Kea shield lavas (45 ± 10) (Huang and Frey, 2003) and OIB (47 ± 10) (Hofmann et al., 1986). East and West Molokai lavas have slightly higher ratios, 56.9 and 51.7, respectively. In contrast, Loa- and Kea-trend lavas typically have

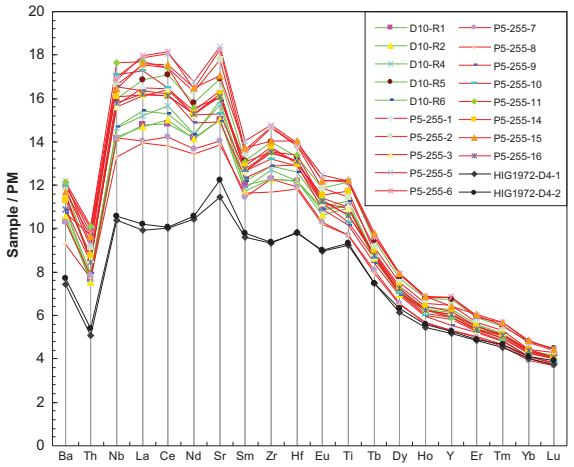

Fig. 5. Primitive mantle-normalized abundances of incompatible elements with the element incompatibility decreasing from left to right. Notable anomalies are high Ba/Th, Sr/Nd and Zr/Sm. Primitive mantle values from McDonough and Sun (1995).

different ratios of Sr/Nb and Zr/Nb (Fig. 6c). Most Penguin Bank lavas have relatively high Sr/Nb and Zr/Nb ratios that are within the field of Mauna Loa lavas; in contrast, samples P5-255-9, -10 and -11 are within the field of Mauna Kea lavas (Fig. 6c).

6.4. Radiogenic isotope ratios of Sr, Nd, Hf and Pb in whole-rocks

Typical of oceanic basalts, $^{87}Sr/^{86}Sr$ and $^{143}Nd/^{144}Nd$ are inversely correlated and $^{143}Nd/^{144}Nd$ and $^{176}Hf/^{177}Hf$ are positively correlated in Penguin Bank lavas. Except for a small region of overlap, these isotopic ratios distinguish Loa- and Kea-trend lavas (Fig. 7a and b). The two HIG1972-D4 samples from Penguin Bank have the most radiogenic $^{87}Sr/^{86}Sr$ and least radiogenic $^{143}Nd/^{144}Nd$ and $^{176}Hf/^{177}Hf$; hence among the Penguin Bank samples they have the strongest Loa-type geochemical signature. Three *Pisces V* dive samples (P5-255-9, -10 and -11 from ~18 km southwest of the HIG dredges, Fig. 1b) plot near the small region of overlap between Loa and Kea lavas (Fig. 7a and b); among the Penguin Bank lavas, they are the only Kea-type lavas.

The $^{208}Pb/^{204}Pb$ vs. $^{206}Pb/^{204}Pb$ plot has been used to discriminate between Loa and Kea shield lavas (Tatsumoto, 1978; Abouchami et al., 2005); specifically Loa-trend volcanoes have higher $^{208}Pb/^{204}Pb$ at a given $^{206}Pb/^{204}Pb$ (see boundary line in Fig. 8a). Shield lavas collected from the flanks of East Molokai Volcano are clearly within the Kea field. In contrast, two of the five samples from the Wailau landslide blocks, possibly older samples of the East Molokai shield derived from the steep headwall on the north side of East Molokai Volcano (Beeson, 1976), are in the Loa field (Fig. 8a). Shield lavas from West Molokai volcano also cross the Loa–Kea boundary line (Fig. 8a). Penguin Bank samples, such as West Molokai lavas, range from the Kea field (dive samples P5-255-9, -10, and -11) to the Loa field (HIG1972-D4 samples), but none of the

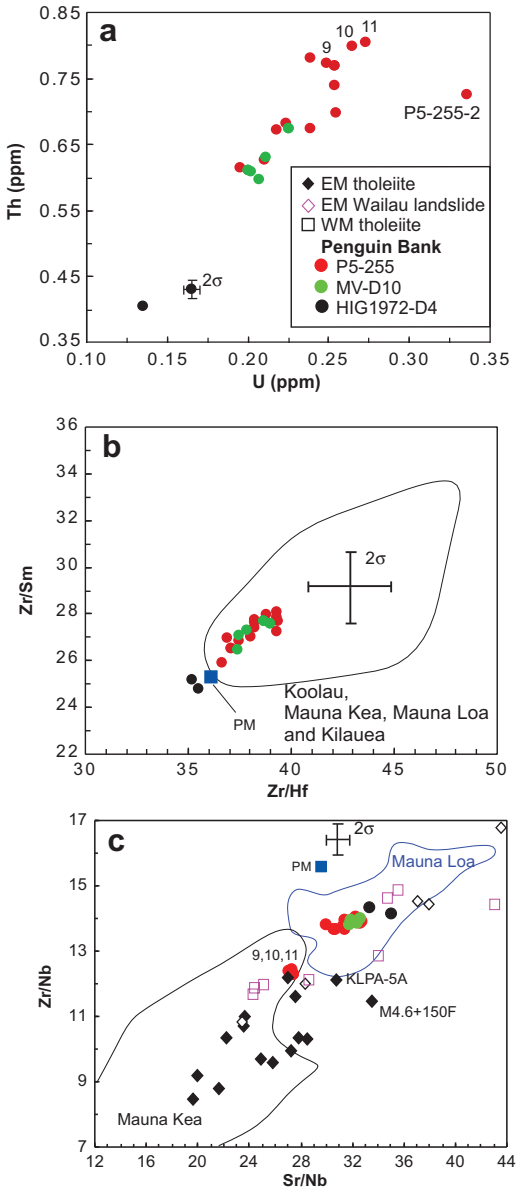

Fig. 6. (a) Th versus U showing a linear trend, except for sample P5-255-2, indicating that U was not highly mobilized by alteration in most of the Penguin Bank samples. The altered samples (low K_2O/P_2O_5 or high Ba/Rb or low Ba/Th) are excluded (see Fig. S1). (b) Zr/Sm vs. Zr/Hf showing that Penguin Bank samples range from PM ratios (HIG samples) to greater than PM ratios. (c) Zr/Nb versus Sr/Nb showing that these ratios distinguish Mauna Loa and Mauna Kea shield lavas. Penguin Bank samples, except for P5-255-9, -10 and, -11, have high Loa-type ratios. Lavas with Loa- and Kea-type ratios were obtained from Wailau landslide blocks that are inferred to be relatively old parts of the East Molokai shield. In panels b and c, only lavas with MgO >6.5% are plotted or used to define the fields to minimize the effects of clinopyroxene, plagioclase, and Fe–Ti oxide fractionation on Sr/Nb, Zr/Nb and Zr/Sm ratios; the primitive mantle values are from McDonough and Sun (1995). The 2σ uncertainties are 5%. *Data sources:* Mauna Kea – Frey et al. (1990, 1991), Rhodes (1996), Huang and Frey (2003), Rhodes et al. (2012); Mauna Loa – Rhodes (1995, 1996), Rhodes and Hart (1995), Rhodes and Vollinger (2004), Morgan et al. (2007); East Molokai Wailau landslide samples – Tanaka et al. (2002); Koolau – Kalihi-stage – Huang and Frey (2005b).

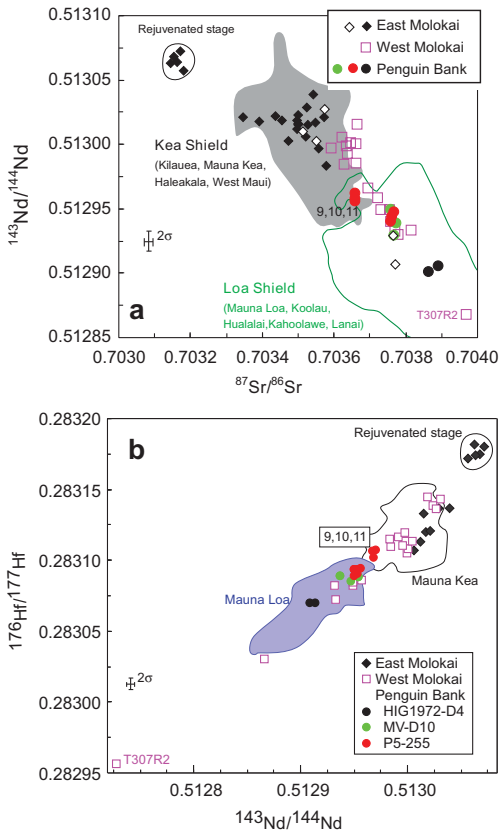

Fig. 7. (a) $^{143}Nd/^{144}Nd$ vs. $^{87}Sr/^{86}Sr$ showing data for East and West Molokai and Penguin Bank lavas and fields for Loa- and Kea-trend volcanoes. East Molokai shield lavas collected from the subaerial slopes of the volcano (filled diamonds) are entirely within the Kea field but submarine samples from the Wailau landslide blocks (unfilled diamonds) include both Kea- and Loa-type lavas; West Molokai shield lavas range from Kea to Loa fields. Most Penguin Bank samples are within the field of Loa shield lavas but samples P5-255-9, -10 and, -11 plot where the Loa- and Kea-type fields overlap. Only acid-leached Sr and Nd isotopic data were used to define fields for Kea and Loa volcanoes. (b) $^{143}Nd/^{144}Nd$ vs. $^{176}Hf/^{177}Hf$ for East and West Molokai and Penguin Bank lavas and fields for Mauna Loa and Mauna Kea shield lavas. As in (a) samples collected from the slopes of East Molokai are in the Kea field, and West Molokai lavas range from the Kea to Loa fields, whereas Penguin Bank samples are within the Mauna Loa field except that the three *Pisces V* samples P5-255-9, -10, and -11 are in the Kea field. *Data sources:* East Molokai – Xu et al. (2005, 2007), Tanaka et al. (2002) and Basu and Faggart (1996); West Molokai – Xu et al. (2007); Hualalai – Sims et al. (1999), Stracke et al. (1999), Stille et al. (1986), Yamasaki et al. (2009); Mauna Loa – Abouchami et al. (2000), Blichert-Toft and Albarède (1999), Cohen et al. (1996), DePaolo et al. (2001), Hauri et al. (1996), Kurz et al. (1995), Marske et al. (2007), Rhodes and Hart (1995), Stracke et al. (1999), Wanless et al. (2006), Weis et al. (2011), Tanaka et al. (2008); Mauna Kea – Abouchami et al. (2000), Blichert-Toft and Albarède (1999, 2009), Blichert-Toft et al. (1999), Bryce et al. (2005), Kennedy et al. (1991), Lassiter et al. (1996); Kilauea – Chen et al. (1996), Marske et al. (2007), Pietruszka and Garcia (1999), Ren et al. (2009); Kahoolawe – West et al. (1987), Huang et al. (2005); Haleakala – Ren et al. (2006); West Maui – Gaffney et al. (2004); Lanai – Gaffney et al. (2005); Koolau – Roden et al. (1994), Blichert-Toft et al. (1999), Ren et al. (2009), Salters et al. (2006).

Penguin Bank samples have Pb isotopic ratios comparable to the extreme Loa end member defined by lavas in the Makapuu stage of Koolau Volcano, the Lanai and Kahoolawe shields, and the submarine sample, T307R2, collected between Koolau and West Molokai Volcanoes (Fig. 8a and c). Both isotopic and trace element ratios (e.g., Zr/Nb vs. Sr/Nb) define distinct fields for Penguin Bank dive samples P5-255-9, -10 and -11 (Kea-type) and the HIG1972-D4 samples (Loa-type) (Figs. 6–8).

In a plot of $^{207}Pb/^{204}Pb$ vs. $^{206}Pb/^{204}Pb$ (Fig. 8b), the two HIG dredge samples are offset from other Penguin Bank samples to low $^{207}Pb/^{204}Pb$ at a given $^{206}Pb/^{204}Pb$. Similarly, three West Molokai samples and four rejuvenated-stage lavas from East Molokai are also offset to low $^{207}Pb/^{204}Pb$. The low $^{207}Pb/^{204}Pb$ ratios in these Penguin Bank and West Molokai samples are coupled with high $^{208}Pb^*/^{206}Pb^*$ ratios ($^{208}Pb^*/^{206}Pb^*$ is defined as $(^{208}Pb/^{204}Pb_{sample} - 29.475)/(^{206}Pb/^{204}Pb_{sample} - 9.3066)$ after Galer and O'Nions (1985), Fig. 8c). On a global scale, Hawaiian shield lavas, including Penguin Bank lavas, define a negative trend in $^{208}Pb^*/^{206}Pb^*$ vs. $^{207}Pb/^{204}Pb$ (Fig. 8c).

7. DISCUSSION

7.1. Ni abundance in olivine phenocrysts and SiO_2 content of Hawaiian shield lavas: Controlled by source and/or process?

The positive correlation between NiO and the forsterite (Fo) contents in olivine phenocrysts of Hawaiian lavas (Fig. 2) reflects the compatibility of Ni and Mg in olivine (e.g., Beattie et al., 1991). At a given Fo content, however, there is considerable variation in the NiO content of olivine, an observation attributed to crystal fractionation and magma mixing (e.g., Clague et al., 1995). Olivine phenocrysts in basalt from the Loa-trend Mauna Loa volcano, and the Kea-trend volcanoes, Kilauea and Mauna Kea, overlap in Ni content at a given Fo (Sobolev et al., 2005). Also, olivine phenocrysts in the high- (Loa-type) and low-SiO_2 (Kea-type) Mauna Kea lavas have similar NiO contents at a given MgO (Fig. 2b) (Putirka et al., 2011). Similarly, Penguin Bank contains both Loa- and Kea-type lavas (as defined by Pb isotopic ratios), and the NiO vs. Fo trends for olivines from the Loa- and Kea-type lavas overlap (Fig. 2a). A difference between Loa- and Kea-type lavas is expected if these types were derived from source rocks with very different mineralogy, such as pyroxenite and peridotite (Sobolev et al., 2005). Clearly, the Ni content of olivine phenocrysts does not distinguish between Loa-and Kea-type lavas. A complication is that the Ni partition coefficient between olivine and melt varies with temperature and melt composition (e.g., Beattie, 1993; Herzberg, 2011; Putirka et al., 2011); consequently, the NiO content of olivine phenocrysts and their whole-rocks will vary during variable extents of partial melting and crystallization. We conclude that the NiO content of olivine phenocrysts is determined by source mineralogy and variable extents of processes such as partial melting and crystal fractionation.

Most shield lavas with Loa-type Pb isotopic ratios have relatively high SiO_2 content at a given MgO content (Loihi

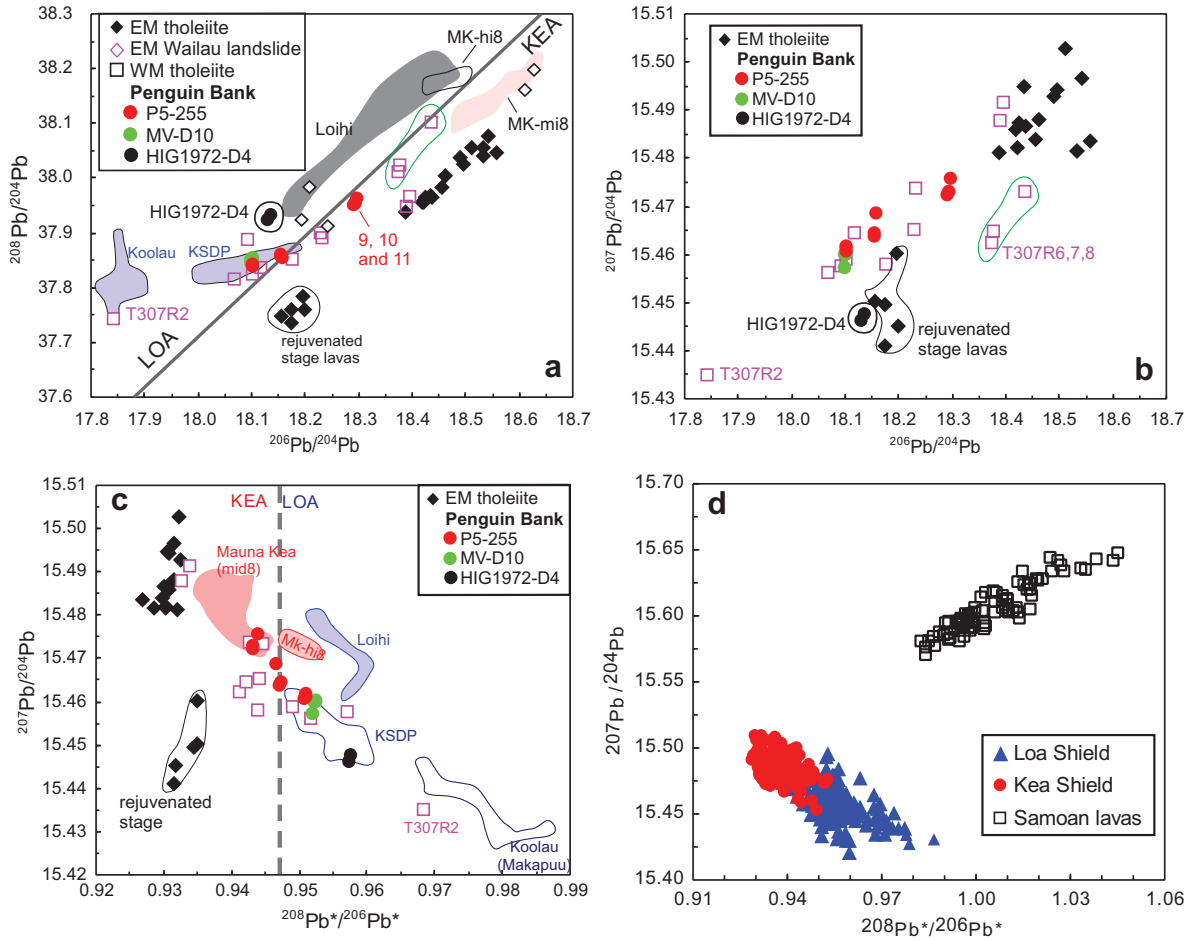

Fig. 8. $^{208}Pb/^{204}Pb$ vs. $^{206}Pb/^{204}Pb$, $^{207}Pb/^{204}Pb$ vs. $^{206}Pb/^{204}Pb$, and $^{208}Pb^*/^{206}Pb^*$ vs. $^{207}Pb/^{204}Pb$. ($^{208}Pb^*/^{206}Pb^*$) is defined as ($^{208}Pb/^{204}Pb$ – 29.475)/($^{206}Pb/^{204}Pb$ – 9.3066) (Galer and O'Nions, 1985). We plot only the precise and accurate data (especially for $^{207}Pb/^{204}Pb$) obtained by the triple spike Pb technique. (a) The black diagonal line is the Loa–Kea dividing line proposed by Abouchami et al. (2005). Except for some samples from Wailua landslide blocks (open diamonds), all East Molokai lavas are in the Kea field, West Molokai samples range from the Kea field to the Loa field, and Penguin Bank lavas, except for samples P5-255-9, -10 and, -11, are in the Loa field. (b) Samples T307R6, 7, and 8 from West Molokai, HIG1972-D4 samples from Penguin Bank, and rejuvenated-stage lavas from East Molokai are offset to low $^{207}Pb/^{204}Pb$ at a given $^{206}Pb/^{204}Pb$. (c) Shield lavas from Koolau (KSDP and Makapuu), Loihi, and Mauna Kea (mid-8 and hi-8 groups defined by Eisele et al. (2003)), West Molokai, and Penguin Bank define a negative trend. One dredged sample from Loihi with very low $^{207}Pb/^{204}Pb$ is not plotted. Loa end member is defined by Makapuu lavas erupted at Koolau volcano. (d) In contrast to the negative trend defined by Hawaiian shield lavas, Samoan lavas define positive trends. Data sources for Hawaiian lavas are listed in the caption of Fig. 7. Samoan data from the compiled data set of Huang et al. (2011).

basalts are an exception), and this correlation has provided evidence for the SiO_2 content of Hawaiian shield lavas being controlled by source mineralogy (Hauri, 1996; Jackson et al., 2012). It is well established, however, that SiO_2 abundance is also controlled by processes such as the depth of melt segregation and extent of melting (e.g., Klein and Langmuir, 1987). Although most shield basalts from Mauna Kea have Kea-type geochemical characteristics, basaltic glasses from the Mauna Kea shield recovered by the Hawaiian Scientific Drilling Project are bimodal in SiO_2 content (Stolper et al., 2004); Penguin Bank glasses are also bimodal in SiO_2 content (Figs. 3a and 4a). Mauna Kea lavas with Loa-type Pb isotopic ratios belong to the low-SiO_2 group; in contrast, Penguin Bank lavas with Loa-type Pb isotopic ratios are in the high-SiO_2 group. We conclude that for these volcanoes the SiO_2 content of their shield lavas is not solely controlled by source composition. Consequently, the effects of processes, such as depth of melt segregation, were probably important in creating the considerable scatter seen in plots of SiO_2 content versus radiogenic isotopic ratios for Hawaiian shield lavas (see for example Fig. 4 of Jackson et al. (2012)).

7.2. Implications arising from the Pb isotopic characteristics of Kea- and Loa-trend shield lavas

The trend of $^{143}Nd/^{144}Nd$ vs. $^{208}Pb^*/^{206}Pb^*$ shows that Kea-trend lavas could be explained by mixing of Loihi and Kea components, whereas Loa-trend lavas could be mixtures of Loihi and the end member Loa component

(Fig. 9). The Pb isotope systematics of Hawaiian shield lavas requires more than two-component mixing. In particular, Loa- and Kea-trend lavas define different Pb isotope arrays that have been interpreted in terms of mixing between various components (Abouchami et al., 2000, 2005; Eisele et al., 2003). As described in Abouchami et al. (2000), whether the $^{207}Pb/^{204}Pb$ vs. $^{206}Pb/^{204}Pb$ array represents an isochron can be evaluated using $^{208}Pb/^{204}Pb$ vs. $^{206}Pb/^{204}Pb$ systematics, whereby the κ, $(^{232}Th/^{238}U)_{today}$, calculated from the ^{208}Pb–^{206}Pb slope using the ^{207}Pb–^{206}Pb age, is compared with κ^*, the measured $^{232}Th/^{238}U$ ratio of the lavas. If κ^* is significantly different from κ, Pb isotope arrays are unlikely to represent isochrons and are better interpreted as mixing lines (Abouchami et al., 2000). In $^{207}Pb/^{204}Pb$ vs. $^{206}Pb/^{204}Pb$, the Penguin Bank lavas define a trend with a slope of 0.0815 corresponding to an "age" of 1.23 Ga (Table S3 and Fig. S2). Measured Th/U ratios in Penguin Bank lavas vary between 2.2 and 3.3, with a mean value of 2.95 ± 0.22 comparable to that reported for other Hawaiian lavas (Hofmann and Jochum, 1996). The slope of the $^{208}Pb/^{204}Pb$ vs. $^{206}Pb/^{204}Pb$ trend yields a κ value of 1.76 (Table S3 and Fig. S2), which is significantly lower than both the $^{232}Th/^{238}U$ ratio ($=\kappa^*$) of 3.1 ± 0.14 recalculated from the measured concentration ratio (omitting outlier sample P5-255-2 with a ratio of 2.23) and the mean value of 3.2 ± 0.4 reported for Hawaiian volcanoes (see compilation in Abouchami et al., 2000). The overall uniformity of κ^* values in Hawaiian lavas suggests that the source $^{232}Th/^{238}U$ ratios are relatively constant (~3.2). Therefore, we suggest that the Penguin Bank Pb isotope array is best explained by mixing between components of various ages

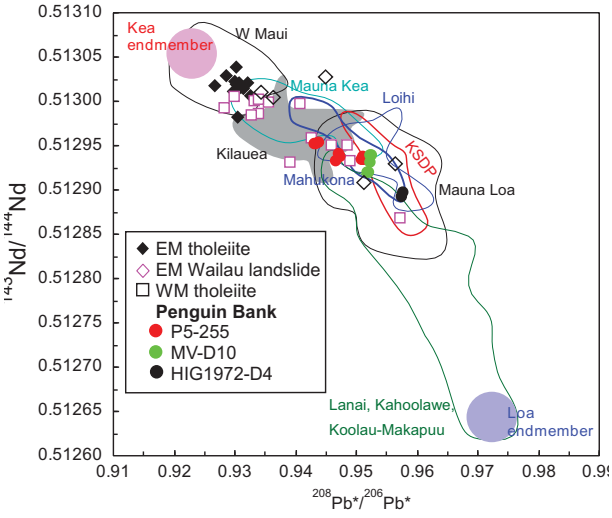

Fig. 9. $^{143}Nd/^{144}Nd$ vs. $^{208}Pb^*/^{206}Pb^*$ showing the extreme Kea component at high $^{143}Nd/^{144}Nd$ and low $^{208}Pb^*/^{206}Pb^*$; Kea shields trend from this Kea component to the Loihi field. The extreme Loa component, defined by the Makapuu lavas at Koolau Volcano, has low $^{143}Nd/^{144}Nd$ and high $^{208}Pb^*/^{206}Pb^*$ (Huang and Frey, 2005b). Loa shields trend from this Loa end member to the Loihi field. As in Figs. 6–8, most East Molokai lavas plot in the Kea field, West Molokai lavas range from the Kea to Loa fields, and Penguin Bank lavas are within the Mauna Loa field except for samples P5-255-9, -10, and -11 which are in the Kilauea field. Data sources are the same as Fig. 7.

from a heterogeneous source. Eisele et al. (2003) reached the same conclusion based on the Pb isotopic data for Mauna Kea shield lavas recovered by the Hawaiian Scientific Drilling Project. Similarly, the discrepant ages inferred from S and Pb isotopes in lavas from Mangaia, Cook Islands, led Cabral et al. (2013) to conclude that the $^{207}Pb/^{204}Pb$–$^{206}Pb/^{204}Pb$ arrays are unlikely to reflect "isochrons".

Another complexity is that relative to the trend of other Penguin Bank samples, the two HIG1972-D4 samples with high $^{208}Pb^*/^{206}Pb^*$ are offset to low $^{207}Pb/^{204}Pb$ at a given $^{207}Pb/^{204}Pb$ (Fig. 8b). These Pb isotopic ratios reflect long-term integrated high Th/U and low U/Pb, respectively. The geochemical differences between Loa- and Kea-type lavas are commonly attributed to variable proportions of oceanic lithosphere (sediment–basalt–gabbro–peridotite) recycled into the mantle in subduction zones. The timing of recycling is important. The end member Loa component, has $^{208}Pb^*/^{206}Pb^*$ of 0.99 (Fig. 8d), close to the primitive mantle value of 0.97 based on Th/U of 3.92 for primitive mantle (Mcdonough and Sun, 1995). This similarity to PM is surprising because the extreme Loa-type component (Makapuu lavas of Koolau shield) has been inferred to be recycled altered oceanic crust containing ancient sediments (Blichert-Toft et al., 1999; Huang and Frey, 2005b). In the present oxidizing environment, U as a 6+ ion is mobile during weathering of continental crust; consequently, river water, seawater, marine sediments, and altered oceanic crust have lower Th/U than primitive mantle. However, in the anoxic Archean environment before 2.5 Ga U was much less mobile (e.g., Farquhar et al., 2000). Consequently, before 2.5 Ga, subducted upper oceanic crust, including sediment, would have $(Th/U)_{PM} \sim 1$, as required to explain the high $^{208}Pb^*/^{206}Pb^*$ signature of Loa-type lavas (Staudigel et al., 1995; Collerson and Kamber, 1999). This Th/U ratio is larger than the 2.5–2.9 of the modern upper mantle (Salters and Stracke, 2004; Workman et al., 2004). In summary, the Loa-type geochemical signature is consistent with ancient subduction, >2.5 Ga, whereas that of the Kea-type might reflect younger subduction, <1.5 Ga, consistent with the Monte-Carlo modeling of the Pb isotope systematics by Eisele et al. (2003).

Samoan volcanoes are located along two sub-parallel spatial arrays (Workman et al., 2004). Huang et al. (2011) found that, like recent Hawaiian volcanoes, Samoan lavas on the southern trend have "Loa-type" characteristics, i.e., higher $^{208}Pb^*/^{206}Pb^*$ and lower $^{143}Nd/^{144}Nd$, than lavas on the northern trend. However, a significant geochemical difference between Samoan and Hawaiian shield lavas is observed in $^{208}Pb^*/^{206}Pb^*$ vs. $^{207}Pb/^{204}Pb$. Hawaiian lavas define a negative correlation, with the high $^{208}Pb^*/^{206}Pb^*$ and low $^{207}Pb/^{204}Pb$ extreme defined by the Loa-type endmember (Makapuu-stage of Koolau in Fig. 8c); this Loa end member reflects time-integrated high Th/U and low U/Pb ratios. In contrast, the positive $^{208}Pb^*/^{206}Pb^*$ vs. $^{207}Pb/^{204}Pb$ trend defined by Samoan lavas (Fig. 8d) requires an end member with time-integrated high Th/U and high U/Pb. The high $^{87}Sr/^{86}Sr$ ratios (up to 0.720) in some Samoan lavas led Jackson et al. (2007) to conclude that recycled marine sediments derived from upper

continental crust (UCC) are present in the source of Samoan lavas. The continental crustal component in the source of Samoan lavas might have been modified during subduction by a fluid component with a very low U/Pb ratio (Kelley et al., 2005), thereby creating a recycled source component with high U/Pb.

7.3. Occurrence of the extreme Loa-Type geochemical component

Tholeiitic basalt with extreme Loa-type geochemical characteristics has erupted northwest of Penguin Bank in Makapuu-stage lavas of the Koolau shield. Southeast of Penguin Bank a similar component contributed to shield lavas at Lanai and Kahoolawe volcanoes (West et al., 1987; Leeman et al., 1994; Basu and Faggart, 1996; Abouchami et al., 2005; Huang et al., 2005). Except for a dredged basaltic sample (T307R2 in Figs. 7 and 8), whose origin may have been Koolau or West Molokai volcano (see Fig. 1c of Xu et al., 2007), none of the shield lavas on Molokai Island or the sparsely sampled Penguin Bank have the geochemical characteristics of the extreme Loa-type component. For the Makapuu-stage of the Koolau shield, the extreme Loa-type composition has been attributed to a $\sim$10 km^3 block of eclogite, i.e., recycled ocean crust, in the hotspot magma source (Fig. 8 of Takahashi and Nakajima, 2002). The presence of this component northwest and southeast of Molokai Island, but its absence at Penguin Bank and rarity at West Molokai volcano, indicates that this extreme Loa-type component is not abundant in time and space (Tanaka et al., 2008).

7.4. Longevity of geochemical differences between the Loa and Kea spatial trends

Jackson et al. (1972, their Fig. 1) terminated the Loa and Kea spatial trends at West and East Molokai volcanoes, respectively. However, Abouchami et al. (2005), using $^{208}Pb^*/^{206}Pb^*$ as the Loa–Kea discriminant, concluded that the geochemical differences between the Loa and Kea spatial trends terminated at Lanai (Loa-trend) and Haleakala (Kea-trend), i.e., southeast of Molokai Island (Fig. 1a); this conclusion was based on Kea-type Pb isotopic data for one landslide sample inferred to be derived from West Molokai (Tanaka et al., 2002), but it may have been derived from the Koolau shield (Garcia, personal communication, 2006). Using the additional Pb isotopic data reported for West and East Molokai volcanoes (Xu et al., 2005, 2007), we can re-assess the spatial extension of the Loa–Kea Pb isotope boundary and more specifically, determine whether the geochemical differences between Kea- and Loa-trend lavas persist as far north as Molokai Island. In particular, we evaluate if there is a transition from Kea- to Loa-type geochemical characteristics in the east to west transect defined by shield lavas from East Molokai, West Molokai, and Penguin Bank volcanoes (Fig. 1a), i.e., northwest of the boundary proposed by Abouchami et al. (2005). Based on our data for Molokai Island volcanoes, we find that each volcano includes lavas with both Loa- and Kea-type geochemical characteristics (Xu et al., 2005). The geochemical heterogeneity of lavas from the West Molokai and Penguin Bank shields precludes using their lava compositions to evaluate the relationship of Penguin Bank to West Molokai. Even with the abundant geochemical data for the 3500 m basaltic drill core recovered from the flank of Mauna Kea Volcano by the Hawaii Scientific Drilling Project, there is considerable debate about how many distinct volcanoes have contributed to this core (see Section 4.4 of Rhodes et al., 2012). However, the proportion of Loa-type lavas increases significantly from East Molokai on the Kea-trend to West Molokai to Penguin Bank, both on the Loa-trend (Fig. 10). Consequently, we conclude that geochemical differences between Loa- and Kea-trend volcanoes persist along the entire length of the Loa and Kea spatial trends and extend beyond the Molokai Fracture Zone; however, there are no Kea-trend volcanoes northwest of East Molokai. In contrast, volcanoes with Loa-type geochemical characteristics continue to the northwest, i.e., the Makapuu stage of the Koolau shield (Roden et al., 1994; Huang and Frey, 2005b) and Kauai (Weis et al., 2011).

7.5. Shields containing lavas with both Loa- and Kea-type geochemical characteristics

In agreement with Abouchami et al. (2005), Weis et al. (2011) emphasized that the geochemical differences between Loa- and Kea-trend volcanoes, especially in Pb isotopic space, are clearly defined with few exceptions. In contrast, we emphasize that several Loa-trend volcanoes, specifically West Molokai, Penguin Bank and Mahukona, contain a significant proportion of lavas with Kea-type geochemical characteristics (Table 7 of Xu et al., 2007; Table 2 of Huang et al., 2013). There are also several examples of Loa-type lavas in Kea-trend volcanoes. Specifically, East Molokai late shield and post-shield lavas have Kea-type Pb isotopic ratios, but the probably older East Molokai shield lavas recovered from Wailau landslide blocks include lavas with both Loa-type and Kea-type Pb isotopic ratios (e.g., Tanaka et al., 2002; Xu et al., 2005); Mauna Kea low-SiO_2 group shield lavas have Loa-type Pb isotopic compositions (e.g., Eisele et al., 2003); two Kohala shield lavas have Pb isotopic ratios similar to Mauna Loa lavas (Fig. 2 of Abouchami et al., 2005); and some of the analyzed late-shield lavas erupted at Haleakala (the Honomanu Volcanics) also have Loa-type Pb isotopic compositions (Abouchami and Frey, 2006; Ren et al., 2006).

Loa-trend volcanoes span a wider range in radiogenic isotopic ratios than Kea-trend volcanoes (Figs. 6b and 7–9), a conclusion also reached by Abouchami et al. (2005) and Weis et al. (2011). This observation is commonly attributed to a larger proportion and diversity of recycled oceanic lithosphere components in the source of Loa-trend volcanoes (e.g., Huang and Frey, 2005b; Huang et al., 2009).

7.6. Distribution of geochemical heterogeneities in the source of Hawaiian shield magmas

Xu et al. (2007) summarized five models that have been proposed to explain the geochemical differences between

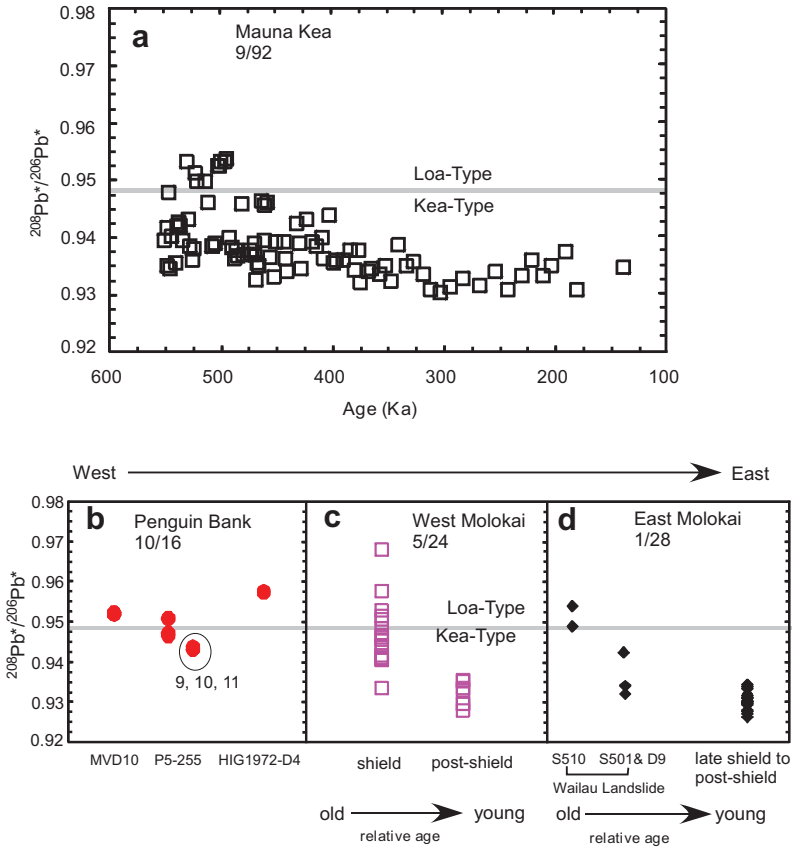

Fig. 10. $^{208}Pb^*/^{206}Pb^*$ vs. eruption age for lavas from Mauna Kea, Penguin Bank, West Molokai and East Molokai. Ages are well constrained for Mauna Kea (Bryce et al., 2005), unconstrained for Penguin Bank lavas, and inferred for samples recovered from the Wailau landslide blocks (Tanaka et al., 2002). Specifically, the landslide blocks are inferred to be older than samples collected from the subaerial shield, and samples collected on Dive S501 from the distal landslide block are inferred to be younger than those collected on Dive S510 closer to the subaerial shield. The ratio (number of Loa-type samples)/total analyzed samples is indicated for the Molokai Volcanoes. Data from Tanaka et al. (2002) and Xu et al. (2005, 2007).

Loa- and Kea-trend lavas. These models involve differences in the proportion, distribution, and size of geochemical heterogeneities in the sources of Hawaiian shield magmas.

A recent model for the zonation in the source of Hawaiian basalt (Pietruszka et al., 2013) is based on Loihi Seamount, a preshield-stage Hawaiian volcano. Although it is on the Loa spatial trend (Fig. 1a), Loihi basalts do not have some of the Loa-type geochemical characteristics, e.g., they do not have the relatively high SiO_2 and low CaO that is typical of Loa-type lavas. In order to explain some chemical similarities between basalts from Kilauea and Loihi volcanoes, Pietruszka et al. (2013) proposed that "the mantle source of the active Hawaiian volcanoes is probably heterogeneous on a small scale with a NW–SE oriented gradient in the amount, type (i.e., basalt vs. gabbro), and extent of dehydration of the ancient recycled oceanic crust". We do not evaluate this model in this paper because our efforts are focused on the oldest portion of the Loa and Kea spatial trends (Fig. 1a) where preshield-stage lavas are not exposed.

Two models shown by Xu et al. (2007) that could explain the geochemical changes in basalt from East Molokai to West Molokai to Penguin Bank are shown in Fig. 11; in panel a, the shield lavas directly reflect a spatially variable proportion of the Loa-type component in their source (Kurz et al., 2004; Abouchami et al., 2005; Herzberg, 2005; Ren et al., 2005). Using the numerical simulation approach of Farnetani and Hofmann (2009), Farnetani et al. (2012) showed how a large-scale gradient in $^{208}Pb^*/^{206}Pb^*$ at the core-mantle boundary can be introduced into the Hawaiian plume conduit and subsequently sampled as Loa- and Kea-type lavas. Their model predicts that: (a) at an individual volcano, $^{208}Pb^*/^{206}Pb^*$ systematically varies with eruption age, i.e., from pre-shield to shield to post-shield-stage lavas and (b) lavas from Loa- and Kea-trend volcanoes will define different trends of $^{208}Pb^*/^{206}Pb^*$ versus eruption age (Fig. 1g and h of Farnetani et al., 2012).

As a test of their modeling, Farnetani et al. (2012) compared the predicted temporal variation of $^{208}Pb^*/^{206}Pb^*$ with measured data for the five shields forming the island of Hawaii. The large short-term variability of $^{208}Pb^*/^{206}Pb^*$ in each shield was not addressed by their modeling; for example, the occurrence of Kea-type lavas in Loa-trend shields and vice versa serve to complicate the trends (see Fig. 4 of Farnetani et al., 2012). The large number of samples defining the temporal trend of Mauna Kea shield lavas

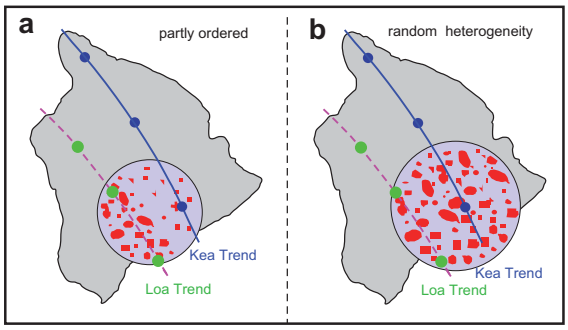

Fig. 11. Two models for explaining Loa and Kea trend geochemical differences (from Fig. 2 of Xu et al. (2007)). (a) The partly ordered zonation model (e.g., Herzberg, 2005) has the proportion of randomly distributed heterogeneities (in red) varying systematically from the Loa to Kea parts of the plume. (b) The randomly distributed heterogeneity model has no systematic zonation (Ren et al., 2005, 2009; Huang and Frey, 2005a). In this model Loa volcanoes sample a higher proportion of heterogeneities with low solidi, perhaps recycled oceanic crust and sediment (red color), whereas Kea volcanoes, which are closer to the plume center, sample a higher proportion of components (blue background) with high solidi, such as peridotites. (For interpretation of the references to color in this figure legend, the reader is referred to the web version of this article.)

provides the best test of model predictions; indeed the overall decrease in $^{208}Pb^*/^{206}Pb^*$ with decreasing eruption age is consistent with model predictions (Fig. 10a of this paper and Fig. 5 of Farnetani et al., 2012).

Farnetani et al. (2012) also compared measured values and model predictions of $^{208}Pb^*/^{206}Pb^*$ in the older Hawaiian shields of West and East Molokai. For these volcanoes, it is important to consider the angle (ϕ) between the direction of Pacific plate motion and the direction of maximum isotopic gradient in the geochemically zoned lower mantle. In the vicinity of the Molokai volcanoes, the strike of the Pacific Plate changed from N65°W for older, 2–3 Ma volcanoes to N30°W for younger Hawaiian volcanoes (Abouchami et al., 2005). This change in plate motion is especially obvious if the Loa spatial trend is drawn through Penguin Bank rather than through West Molokai (Fig. 1a). Fig. 7 of Farnetani et al. (2012) shows that as ϕ decreases from 90° to 0°, the differences in $^{208}Pb^*/^{206}Pb^*$ between Loa- and Kea-trend volcanoes diminish. The available data are not sufficient to test this prediction.

Using $^{208}Pb^*/^{206}Pb^*$ to define Loa- and Kea-type compositions, Fig. 1g of Farnetani et al. (2012) shows that $^{208}Pb^*/^{206}Pb^*$ ratios in Loa-trend shield lavas are greater than in pre- and post-shield lavas. The decrease in $^{208}Pb^*/^{206}Pb^*$ from West Molokai shield to postshield lavas is consistent with this prediction (Fig. 14b, this paper; Fig. 1g of Farnetani et al., 2012). Kea-trend lavas are expected to progressively decrease in $^{208}Pb^*/^{206}Pb^*$ as a volcano evolves from pre-shield to post-shield volcanism. However, Fig. 6d of Farnetani et al. (2012) shows that $^{208}Pb^*/^{206}Pb^*$ in East Molokai lavas increases from late shield/post-shield to rejuvenated stages. This trend is inconsistent with their prediction for a Kea-trend volcano, but was explained as the result of a change in ϕ from 63° to 90° (Farnetani et al., 2012). However, the East Molokai data plotted in Fig. 6d of Farnetani et al. (2012) are misleading because (1) data for five samples from the Wailau landslide deposits, probably derived from old East Molokai shield, were not plotted and (2) inclusion of East Molokai rejuvenated-stage samples, which erupted ~0.8 Ma after shield building (Ozawa et al., 2005), may not be appropriate for their modeling because the sources of rejuvenated-stage lavas differ significantly from those contributing to shield-stage lavas (e.g., Chen and Frey, 1985; Fekiacova et al., 2007; Hofmann and Farnetani, 2013). If we restrict evaluation of the temporal trends of East Molokai lavas to shield and postshield lavas, there is a decrease in $^{208}Pb^*/^{206}Pb^*$ with decreasing age (Fig. 10d, this paper) as predicted for Kea-type volcanoes (Fig. 6d of Farnetani et al., 2012). Consequently, our Pb isotopic data for the transect across the Loa- and Kea-trend defined by the three Molokai volcanoes are consistent with the geochemically zoned model of Abouchami et al. (2005) and Farnetani et al. (2012), without introducing a change in the angle between the direction of Pacific plate motion and the direction of maximum isotopic gradient Hawaiian plume. An unexplained result, however, is the much smaller range of $^{208}Pb^*/^{206}Pb^*$ in lavas from Penguin Bank compared to the variability in West and East Molokai lavas (Fig. 10). Limited variability of $^{208}Pb^*/^{206}Pb^*$ is expected of a centrally located volcano, that is between the Loa and Kea spatial trends (Fig. 7c of Farnetani et al., 2012), but Penguin Bank is the most westerly volcano along the transect. A possible explanation is a larger magma capture zone in the source of Penguin Bank lavas (see Fig. 10 of Huang et al., 2013).

Our results show that from east to west across the strike of the Hawaiian Ridge in the vicinity of Molokai Island, the proportion of Loa-type lavas increases from 3% at East Molokai to 21% at West Molokai, reaching 62% at Penguin Bank (Fig. 10), a result consistent with the asymmetrically zoned plume (Fig. 11a, this paper; Fig. 3b of Abouchami et al., 2005, and Fig. 7 of Farnetani et al., 2012).

A very different model arises from the recognition that different components in the mantle source of Hawaiian lavas will have different solidi (Sleep, 1984; Morgan and Morgan, 1999; Ito and Mahoney, 2005). Therefore, the temperature of the plume at the location of the volcano will control the proportion of components sampled by the volcano. Several studies (Huang and Frey, 2005a; Ren et al., 2006; Tanaka et al., 2008) have proposed that Kea-trend volcanoes, constructed over the relatively hot central part of the plume, contain a high proportion of source components with relatively high solidi, such as peridotite. In contrast, Loa-trend volcanoes formed distant from the plume center at lower temperatures contain a high proportion of components with relatively low solidi, such as pyroxenites formed from subducted oceanic crust. A supporting observation for this model is that Haleakala and Koolau volcanoes evolved from Kea-type shield lavas to Loa-type late shield lavas (Huang and Frey, 2005a; Abouchami and Frey, 2006; Ren et al., 2006; Fekiacova et al., 2007).

Hofmann and Farnetani (2013) criticized the conclusion that Kea-type lavas formed by a higher extent of melting than Loa-type lavas because Kilauea lavas have higher

La/Yb than Mauna Loa lavas. Assuming similar La/Yb in the sources of Kea- and Loa-type lavas, the higher La/Yb of Kilauea lavas reflects a lower extent of melting thereby suggesting that Kea-type lavas did not form at the relatively hot plume center. Fig. 12a shows that for a given shield there is a significant range of Zr/Nb at a given $^{143}Nd/^{144}Nd$. For example, Kilauea lavas have relatively constant $^{143}Nd/^{144}Nd$, but their Zr/Nb ranges from 7.5 to 12.9, with an average of 10.0 ± 1.1 (1σ). This behavior can be interpreted as control by variable extents of melting. However, if the mean Zr/Nb and $^{143}Nd/^{144}Nd$ are calculated for each shield, there is an inverse correlation suggesting that high Zr/Nb is associated with low $^{143}Nd/^{144}Nd$. The plot of La/Yb vs. $^{143}Nd/^{144}Nd$ for several shields (Fig. 12b) has much more scatter, suggesting that La/Yb was dominantly controlled by different extents of melting. However, lavas from the Mauna Loa and Penguin Bank shields show a strong La/Yb vs. $^{143}Nd/^{144}Nd$ correlation consistent with control by source composition (Fig. 12c).

If volcanoes with dominantly Kea-type lavas formed closer to the relatively hot center of the plume than volcanoes with dominantly Loa-type lavas, the temperatures of primary Kea-type magmas should be higher than temperatures of primary Loa-type magmas. These estimates are commonly made for calculated primary melt compositions (e.g., Putirka, 2008; Lee et al., 2009). Typically, a primary melt composition is estimated by adding equilibrium olivine to a parental magma or melt until the MgO content is 16% or the melt composition is in equilibrium with olivine of Fo_{90} (e.g., Jackson et al., 2012). The difficulty with this approach is the choice of parental melt. In contrast to whole-rocks, glass unequivocally was a melt; therefore glass compositions should be the best choice. However, most glasses in Penguin Bank samples are highly evolved, <7% MgO (Table S2 and Fig. 4), and saturated with clinopyroxene and plagioclase, as well as olivine, thereby complicating the calculation of a parental melt composition. In contrast, MV-D11 glasses contain 7.4–10% MgO (Table S2 and Fig. 4) and may be saturated only with olivine. We selected MV-D11 #6, the glass with the highest MgO content and a Loa-type Al_2O_3/TiO_2 ratio, as a parental magma composition (Table 4).

Whole-rocks obtained from Penguin Bank commonly range to high, >10%, MgO (Figs. 3 and 4a; Table 1), but whole-rocks may be mixtures or cumulates rather than melts (e.g., Clague et al., 1995; Rhodes and Vollinger, 2004). An important result for Penguin Bank glasses is that, like Mauna Kea glasses (Stolper et al., 2004), they form two compositional clusters with different SiO_2 contents (Figs. 3, 4a and 13). In order to evaluate the possibility that some Penguin Bank whole-rocks represent parental melt composition for the evolved glasses, we calculated liquid lines of descent using the MELTS web applet (Ghiorso and Sack, 1995) and varied the water content and oxygen fugacity, which controls Fe^{+3}/Fe^{+2}, over a reasonable range. We find that high-SiO_2 whole-rock compositions, such as P5-255-7, P5-255-8, and the two HIG1972-D4 samples, which all have Loa-type geochemical characteristics, evolved via fractional crystallization to the high-SiO_2 glass cluster. Similarly, the whole-rock compositions of Kea-type samples P5-255-9, -10, and -11 evolved to the low-SiO_2 glass cluster (Fig. 13).

We used thermobarometers appropriate for basaltic melt in equilibrium with Fo_{90} olivine (Beattie, 1993; Putirka, 2008; Lee et al., 2009) to calculate temperatures for Penguin Bank primary lavas with Loa- and Kea-type compositions (Table 4). Because olivine is the only crystallizing phase at >7% MgO (Fig. 4), equilibrium olivine, using $Kd^{ol-liq}_{Fe-Mg} = 0.33$ (Matzen et al., 2011), was added incrementally to selected parental melt compositions until the inferred primary magma composition was in equilibrium

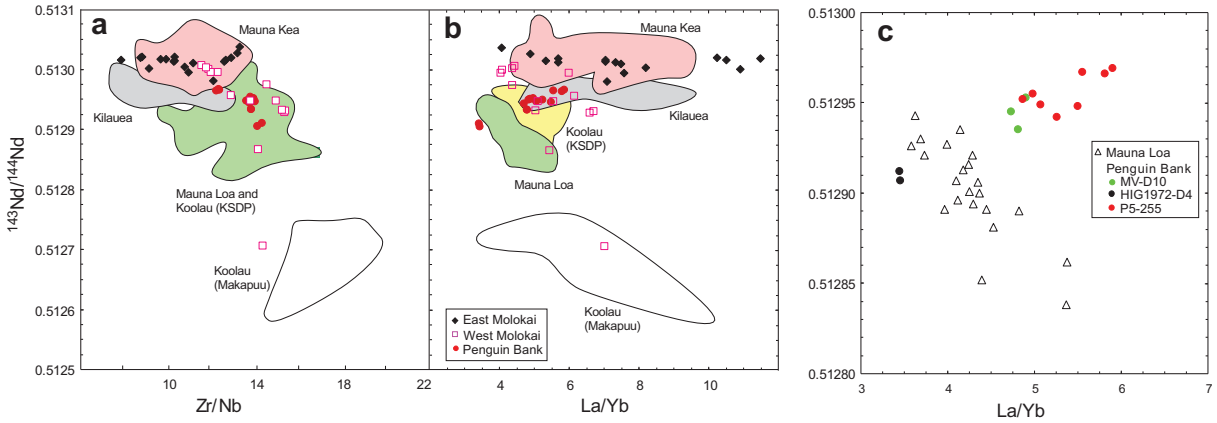

Fig. 12. Zr/Nb and La/Yb vs. $^{143}Nd/^{144}Nd$: (a) and (b) The fields formed by shield lavas from Mauna Kea, Kilauea, East Molokai, and West Molokai have varying Zr/Nb at constant $^{143}Nd/^{144}Nd$ thereby implying that Zr/Nb is controlled by process rather than source, but the average Zr/Nb for each shield varies inversely with $^{143}Nd/^{144}Nd$, thereby providing evidence for control by both process and source. In contrast La/Yb does not correlate with $^{143}Nd/^{144}Nd$ in most of the shields or between shields. Panel c shows, however, that La/Yb is correlated with $^{143}Nd/^{144}Nd$ in lavas from Mauna Loa and Penguin Bank. Although the correlation is negative and positive, respectively, the trends are consistent with La/Yb being controlled by source rather than extent of melting. *Data sources:* Mauna Kea – Huang and Frey (2003), Rhodes et al. (2012); Kilauea – Pietruszka and Garcia (1999) and Chen et al. (1996); Mauna Loa – Rhodes and Hart (1995) and Cohen et al. (1996); Koolau – Huang and Frey (2005b) and Fekiacova et al. (2007).

Table 4
Calculated temperatures for Loa- and Kea-type primary magmas.

	Lee et al. (2009) (assuming 0.5 wt% H_2O)		Lee et al. (2009) (assuming no H_2O)		Putirka (2008) (assuming 0.5 wt% H_2O)	Putirka (2008) (assuming no H_2O)	Beattie (1993) (assuming no H_2O)	Original MgO
	T (°C) Eqn. 3	P (GPa) Eqn. 2	T (°C) Eqn. 3	P (GPa) Eqn. 2	T (°C) Eqn. 22	T (°C) Eqn. 22	T (°C)	wt%
Kea-type Penguin Bank lavas								
P5-255-9	1496	2.49	1512	2.53	1531	1547	1584	15.40
P5-255-10	1484	2.37	1501	2.40	1523	1539	1573	14.89
P5-255-11	1480	2.36	1501	2.44	1522	1540	1575	13.99
Loa-type Penguin Bank lavas								
P5-255-7	1473	2.11	1490	2.14	1504	1520	1549	15.85
P5-255-8	1471	2.14	1488	2.17	1505	1521	1551	15.77
HIG1972-D4-1	1442	1.83	1461	1.88	1479	1495	1519	12.10
HIG1972-D4-2	1443	1.86	1457	1.87	1477	1491	1515	11.47
MV-D11-R1 #5 (glass)	1431	1.64	1449	1.68	1465	1480	1501	10.05
Mauna Loa								
1843	1453	1.93	1468	1.94	1488	1502	1528	13.43
1880	1442	1.64	1457	1.65	1472	1486	1508	13.20
1852	1437	1.71	1451	1.71	1470	1484	1507	13.03
1868	1437	1.68	1451	1.68	1468	1482	1504	13.04
Kea-type Mauna Kea								
SR0490-1.50	1484	2.15	1503	2.18	1504	1519	1546	17.93
SR0574-1.90	1484	2.20	1503	2.24	1505	1521	1549	18.56
SR0582-10.00	1492	2.28	1512	2.33	1510	1526	1555	19.62
SR0683-5.75	1495	2.23	1515	2.28	1510	1526	1554	19.55
SR0916-1.15	1497	2.22	1515	2.25	1514	1530	1558	16.53
SR0939-18.10	1479	2.11	1497	2.14	1501	1516	1543	17.50
SR0954-8.00	1481	2.17	1500	2.21	1504	1519	1548	18.15
R155 (2.7-3.5)	1486	2.09	1504	2.12	1502	1517	1543	17.42
Kilauea								
S492-4	1519	2.57	1538	2.63	1541	1558	1594	18.22
S492-5	1511	2.53	1530	2.58	1537	1554	1590	17.75
S492-6	1470	2.13	1488	2.15	1497	1512	1539	16.50
EK80-77	1505	2.47	1524	2.52	1531	1548	1582	17.98
57-11a (glass)	1455	1.90	1475	1.96	1485	1501	1527	14.60
57-11c (glass)	1522	2.50	1538	2.54	1547	1563	1599	13.20
57-13 (glass)	1495	2.24	1512	2.27	1520	1536	1567	14.80
57-14a (glass)	1454	1.88	1474	1.94	1483	1500	1525	14.60
57-30 (glass)	1460	1.92	1476	1.94	1489	1503	1529	14.70
57-5c (glass)	1469	2.05	1486	2.07	1498	1513	1540	14.70
57-7a (glass)	1464	1.95	1481	1.97	1490	1505	1530	15.00

1. Primary magma compositions were determined by selecting whole-rock or glass compositions whose MgO content is indicated in table as "Original MgO". The sources of selected whole-rock and glass are:
For Penguin Bank samples see text Section 7.6.
For Mauna Loa samples see Rhodes (1995).
For Kea-type Mauna Kea samples see Rhodes and Vollinger (2004).
For Kilauea whole-rock samples see Chen et al. (1996) and Ren et al. (2009), and Kilauea glasses from Clague et al. (1995).
For Mauna Kea and Kilauea whole-rock samples, only samples with isotopic compositions available and MgO contents between 16% and 20% are selected for illustration.
2. Olivine was added to the parental magmas until they are in equilibrium with Fo90 following the slightly different procedures of Lee et al. (2009) and Putirka (2008). In Lee et al. model, the olivine composition in equilibrium with whole-rock is used whereas in Putirka and Beattie's calculations a constant Fo90 olivine is used. The pressure from Lee's model is used in Putirka and Beattie's calculations. $Kd^{ol-liq}_{(Fe-Mg)} = 0.33$ and $Fe^{3+}/Fe^{T} = 0.1$ are used in all calculations.
3. In Lee et al. (2009) calculations, the temperature and pressure calculated using their original equations (Eqn.) 3 and 2, and in Putirka (2008) the equation 22 and pressure calculated from Lee et al. are used to calculate the temperature.

with olivine of Fo_{90}; the highest measured Fo for olivine in Penguin Bank lavas is Fo_{89}. Assuming that primary magmas of Loa- and Kea-types had similar water contents of 0.0% or 0.5%, each equation used to calculate temperature yields higher temperature for Kea-type lavas than for Loa-type lavas (Table 4).

A similar result is found for volcanoes on the Island of Hawaii. Kea-type lavas from Kilauea and Mauna Kea have

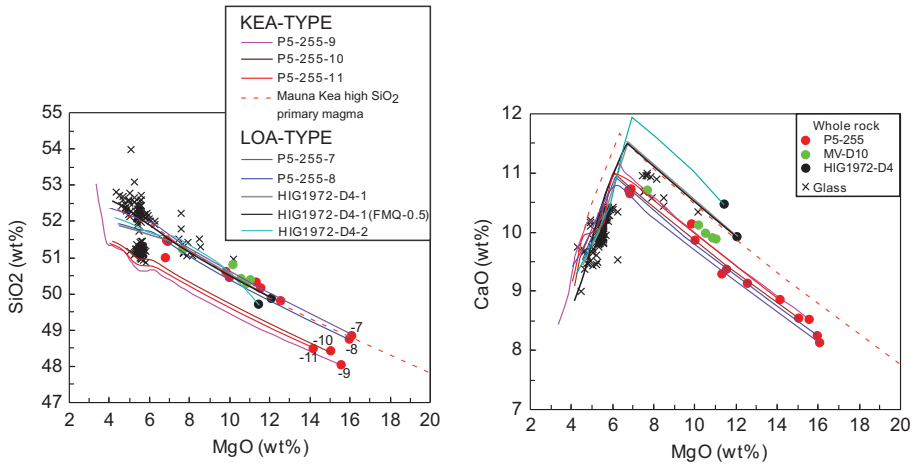

Fig. 13. SiO_2 and CaO vs. MgO showing liquid lines of descent (LLD) calculated using MELTS (Ghiorso and Sack, 1995) and assuming that Penguin Bank whole-rock compositions represent melt compositions. Major element contents were adjusted assuming a $Fe^{3+}/(Fe^{2+} + Fe^{3+})$ molar ratio of 0.10. Calculations assume 0.5% H_2O water in the source and the oxygen fugacity is FMQ-2 except for a second LLD calculated at FMQ-0.5 for HIG1972-D4-1. The linear part of the LLDs at >7% MgO is olivine-dominated fractionation. In panel (a) one LLD extends to <4% MgO and shows the onset of titanomagnetite fractionation. In panel (b) the abrupt decrease in CaO with decreasing MgO reflects clinopyroxene ± plagioclase-dominated fractionation. Samples P5-255-7, -8, and the two HIG samples have Loa-type geochemical characteristics, whereas P5-255-9, -10, and -11 are Kea-type. Glass compositions with <7% MgO are bimodal in SiO_2, and the LLD for Loa-type samples intersect the high-SiO_2 field, whereas the LLD for Kea-type samples intersect the low SiO_2 field. The MV D-11 glasses with 7.4–10% MgO lie along the LLD for Loa-type compositions. Mauna Kea high-SiO_2 primary magma data is from Feigenson et al. (2003).

higher temperatures than Loa-type lavas from Mauna Loa (Table 4). This result, however, conflicts with the inference based on La/Yb that Kilauea lavas were generated via smaller extents of partial melting than Mauna Loa lavas (Hofmann and Farnetani, 2013).

Regardless of the equations used to calculate the temperature of primary Penguin Bank magmas, the temperatures correlate positively with $^{143}Nd/^{144}Nd$, and negatively with $^{208}Pb^*/^{206}Pb^*$. Although there is more scatter in Fig. 14 for primary magmas from Mauna Loa, Mauna Kea and Kilauea, the Loa-type lavas erupted on Mauna Loa have lower temperature and $^{143}Nd/^{144}Nd$ and higher $^{208}Pb^*/^{206}Pb^*$ than Kea-type lavas from Kilauea and Mauna Kea. We conclude that formation of Loa- and Kea-type magmas from an unzoned but heterogeneous source with volcanoes having dominantly Kea-type lavas forming closer to the hot center of the plume than volcanoes with dominantly Loa-type lavas is a viable alternative to a spatially zoned heterogeneous source.

8. CONCLUSIONS

East Molokai, West Molokai, and Penguin Bank volcanoes constructed at ~1.5 to 2 Ma form a nearly east to west trend that crosses at a high angle the Loa- and Kea-spatial trends defined by Hawaiian volcanoes. Lavas erupted at these volcanoes show that the distinct geochemical differences between Loa- and Kea-trend volcanoes have persisted for 2 Ma, i.e., from formation of the East Molokai, West Molokai, and Penguin Bank shields to the ongoing formation of the Mauna Loa and Kilauea shields. The geochemical differences between Loa-and Kea-type lavas, expressed in abundance ratios of major and particularly incompatible trace elements and isotopic ratios of Sr, Nd, Hf, and Pb, reflect geochemical characteristics of the source. However, the relatively high Ni and SiO_2 contents of Loa-trend shield lavas reflect control by both the magma source and the processes that formed the magma. The extreme Loa geochemical component is erratically distributed; it is uncommon or perhaps absent at West Molokai and Penguin Bank but abundant to the northwest (Koolau Volcano) and to the southeast (Lanai and Kahoolawe volcanoes). It has the geochemical signature of ancient (>2.5 Ga) upper oceanic crust.

Although most lavas in Loa- and Kea-trend shields display significant geochemical differences, it is not unusual for lavas with Loa-type geochemical characteristics to occur at Kea-trend volcanoes and vice versa. Each of the Molokai volcanoes erupted lavas with Loa- and Kea-type geochemical characteristics. East Molokai on the Kea trend dominantly erupted Kea-type lavas and Penguin Bank on or west of the Loa trend has dominantly erupted Loa-type lavas. The occurrence of both Loa- and Kea-type lavas in the same volcano constrains models for the spatial distribution of these components.

Two plausible explanations are:

(1) The magma sources for Loa trend and Kea trend volcanoes contain the source components for both Loa-type and Kea-type lavas. However, the proportion of these components is spatially zoned with Loa trend and Kea trend volcanoes sampling source regions with different proportions of Loa-type and Kea-type components.

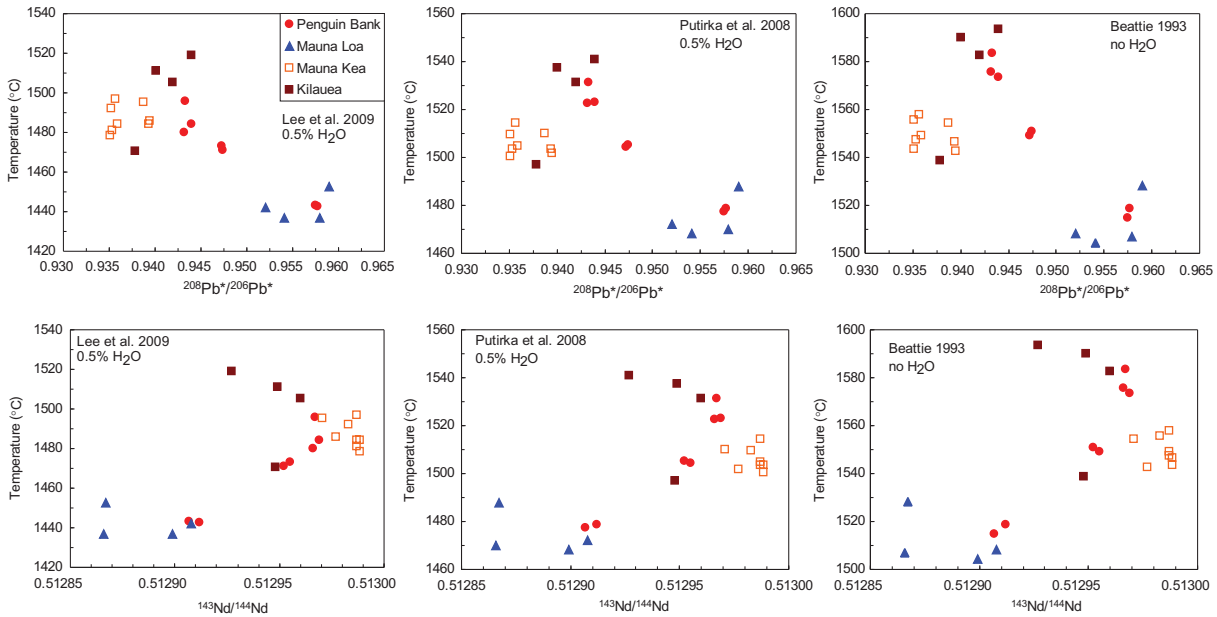

Fig. 14. $^{143}Nd/^{144}Nd$ and $^{208}Pb^*/^{206}Pb^*$ ratios vs. calculated mantle temperature for calculated primary magmas for selected lavas from Penguin Bank, Mauna Loa, and Mauna Kea (Table 4). The temperatures for Penguin Bank lavas are correlated with $^{143}Nd/^{144}Nd$ and $^{208}Pb^*/^{206}Pb^*$ ratios. Shown for comparison are data for primary magmas from Kilauea, Mauna Kea and Mauna Loa Volcanoes (Table 4) Overall, Loa-type lavas have lower temperatures than Kea-type lavas. Mauna Kea data from Rhodes and Vollinger (2004) and Eisele et al. (2003), Kilauea whole-rock data from Chen et al. (1996), Abouchami et al. (2000) and Ren et al. (2009), and Mauna Loa data from Rhodes (1995) and Rhodes and Hart (1995) and Weis et al. (2011).

(2) The sources for Loa- and Kea-trend volcanoes have similar proportions of Loa-type and Kea-type compositional heterogeneities, but these components have different solidi. Consequently, the component with the lower solidus, presumably the Loa component, is preferentially sampled at the relatively cool plume periphery.

Important objectives for the future are to test these alternative models and to understand the processes that created the distinctive Loa- and Kea-type geochemical characteristics.

ACKNOWLEDGMENTS

G.X. thanks Frank Dudas for his help with the Sr isotope analyses. Sam Bowring is thanked for providing financial support for seven Sr isotopic analyses at MIT. Rick Kayser is thanked for his assistance with ICP-MS analysis. The HIG1972-D4 dredge samples were kindly made available to D.A.C. by chief scientist Frisbee Campbell; the Pisces V dive 255 samples were collected during a dive funded by the Hawaii Undersea Research Program of NOAA to D.A.C. and J.G.M., with special thanks to chief pilot Terry Kerby; and the MV-D10 and MV-D11 samples were dredged by D.A.C. during the NSF-funded Plume Program, Gabi Laske, chief Scientist on the R/V Melville. J.B.T. received support from the French Agence Nationale de la Recherche (Grant ANR-10-BLAN-0603M&Ms — Mantle Melting — Measurements, Models, Mechanisms). Research at MIT was supported by NSF Grant EAR-0607895. W.A. was supported by the DFG and through the Leibniz award to Klaus Mezger. D.A.C. was supported by a grant to MBARI from the David and Lucile Packard Foundation. S.H. acknowledges support from NSF grant EAR 1144727. We thank K. Putirka for assistance in calculating temperatures, A. Hofmann for discussion regarding this paper, and M. Jackson, A. Pietruszka, and an anonymous reviewer for their constructive comments that improved the paper.

APPENDIX A. SUPPLEMENTARY DATA

Supplementary data associated with this article can be found, in the online version, at http://dx.doi.org/10.1016/j.gca.2014.02.002.

REFERENCES

Abouchami W. and Frey F. A. (2006) Temporal evolution of Pb isotopes in shield lavas from Haleakala Volcano. *Geophys. Res. Abstr.* **8**.

Abouchami W., Galer S. J. G. and Hofmann A. W. (2000) High precision lead isotope systematics of lavas from the Hawaiian Scientific Drilling Project. *Chem. Geol.* **169**, 187–209.

Abouchami W., Hofmann A. W., Galer S. J. G., Frey F. A., Eisele J. and Feigenson M. (2005) Lead isotopes reveal bilateral asymmetry and vertical continuity in the Hawaiian mantle plume. *Nature* **434**, 851–856.

Basu A. R. and Faggart B. E. (1996) Temporal isotopic variations in the Hawaiian mantle plume: the Lanai anomaly, the Molokai Fracture Zone and a seawater-altered lithospheric component in Hawaiian volcanism. In *Earth Processes: Reading the Isotopic Code* (eds. A. R. Basu and S. R. Hart). Geophysical Monograph, AGU, Washington, D.C., pp. 149–159.

Beattie P. (1993) Olivine-melt and orthopyroxene-melt equilibria. *Contrib. Mineral. Petrol.* **115**, 103–111.

Beattie P., Ford C. and Russell D. (1991) Partition coefficients for olivine-melt and orthopyroxene-melt systems. *Contrib. Mineral. Petrol.* **109**, 212–224.

Beeson M. H. (1976) Petrology, minerlogy, and geochemistry of the East Molokai volcanic series. *US Geol. Surv. Prof. Pap.* **961**, 1–53.

Blichert-Toft J. and Albarède F. (1999) Hf isotopic compositions of the Hawaii Scientific Drilling Project core and the source mineralogy of Hawaiian basalts. *Geophys. Res. Lett.* **26**, 935–938.

Blichert-Toft J. and Albarède F. (2009) Mixing of isotopic heterogeneities in the Mauna Kea plume conduit. *Earth Planet. Sci. Lett.* **282**, 190–200.

Blichert-Toft J., Chauvel C. and Albarède F. (1997) Separation of Hf and Lu for high-precision isotope analysis of rock samples by magnetic sector multiple collector ICP-MS. *Contrib. Mineral. Petrol.* **127**, 248–260.

Blichert-Toft J., Frey F. A. and Albarède F. (1999) Hf isotope evidence for pelagic sediments in the source of Hawaiian basalts. *Science* **285**, 879–882.

Bryce J. G., DePaolo D. J. and Lassiter J. C. (2005) Geochemical structure of the Hawaiian plume: Sr, Nd, and Os isotopes in the 2.8 km HSDP-2 section of Mauna Kea volcano. *Geochem. Geophys. Geosyst.* **6**. http://dx.doi.org/10.1029/2004GC000809.

Cabral R. A., Jackson M. G., Rose-Koga E. F., Koga K. T., Whitehouse M. J., Antonelli M. A., Farquhar J., Day J. M. D. and Hauri E. H. (2013) Anomalous sulphur isotopes in plume lavas reveal deep mantle storage of Archaean crust. *Nature* **496**, 490–493.

Chauvel C. and Blichert-Toft J. (2001) A hafnium isotope and trace element perspective on melting of the depleted mantle. *Earth Planet. Sci. Lett.* **190**, 137–151.

Chen C. Y. and Frey F. A. (1985) Trace-element and isotopic geochemistry of lavas from Haleakala Volcano, East Maui, Hawaii – implications for the origin of Hawaiian basalts. *J. Geophys. Res. Solid Earth Planets* **90**, 8743–8768.

Chen C. Y., Frey F., Rhodes J. M. and Easton R. M. (1996) Temporal geochemical evolution of Kilauea volcano: comparison of Hilina and Puna basalt. In *Earth Processes: Reading the Isotopic Code* (eds. A. Basu and S. R. Hart). Geophysical Monograph, AGU, Washington, D.C., pp. 161–181.

Clague D. A. and Sherrod D. R. The growth and degradation of Hawaiian volcanoes. *US Geol. Surv. Prof. Paper 1801*, in press.

Clague D. A., Moore J. G., Dixon J. E. and Friesen W. B. (1995) Petrology of submarine lavas from Kilaueas Puna Ridge, Hawaii. *J. Petrol.* **36**, 299–349.

Cohen A. S., ONions R. K. and Kurz M. D. (1996) Chemical and isotopic variations in Mauna Loa tholeiites. *Earth Planet. Sci. Lett.* **143**, 111–124.

Collerson K. D. and Kamber B. S. (1999) Evolution of the continents and the atmosphere inferred from Th–U–Nb systematics of the depleted mantle. *Science* **283**, 1519–1522.

Cousens B. L., Clague D. A. and Sharp W. D. (2003) Chronology, chemistry, and origin of trachytes from Hualalai Volcano, Hawaii. *Geochem. Geophys. Geosyst.* **4**. http://dx.doi.org/10.1029/2003GC000560.

David K., Schiano P. and Allègre C. J. (2000) Assessment of the Zr/Hf fractionation in oceanic basalts and continental materials during petrogenetic processes. *Earth Planet. Sci. Lett.* **178**, 285–301.

Davis A. S., Clague D. A. and Friesen W. F. (1994) Petrology and mineral chemistry of basalt from Escanaba Trough, southern Gorda Ridge. *US Geol. Surv. Bull.* **2022**, 153–170.

DePaolo D. J., Bryce J. G., Dodson A., Shuster D. L. and Kennedy B. M. (2001) Isotopic evolution of Mauna Loa and the chemical structure of the Hawaiian plume. *Geochem. Geophys. Geosyst.* **2**. http://dx.doi.org/10.1029/2000GC000139.

Eakins B. W., Robinson J. E., Kanamatsu T., Naka J., Smith J. R., Takahashi E. and Clague D. A. (2003) Hawaiian Volcanoes revealed. *Eos Trans. AGU* **84**(52) (Fall Meet. Suppl.).

Eisele J., Abouchami W., Galer S. J. G. and Hofmann A. W. (2003) The 320 kyr Pb isotope evolution of Mauna Kea lavas recorded in the HSDP-2 drill core. *Geochem. Geophys. Geosyst.* **4**. http://dx.doi.org/10.1029/2002GC000339.

Farnetani C. G. and Hofmann A. W. (2009) Dynamics and internal structure of a lower mantle plume conduit. *Earth Planet. Sci. Lett.* **282**, 314–322.

Farnetani C. G., Hofmann A. W. and Class C. (2012) How double volcanic chains sample geochemical anomalies from the lowermost mantle. *Earth Planet. Sci. Lett.* **359–360**, 240–247.

Farquhar J., Bao H. M. and Thiemens M. (2000) Atmospheric influence of Earth's earliest sulfur cycle. *Science* **289**, 756–758.

Feigenson M. D., Hofmann A. W. and Spera F. J. (1983) Case studies on the origin of basalt II, the transition from tholeiitic to alkalic volcanism on Kohala Volcano, Hawaii. *Contrib. Mineral. Petrol.* **V84**, 390–405.

Feigenson M. D., Bolge L. L., Carr M. J. and Herzberg C. T. (2003) REE inverse modeling of HSDP2 basalts: evidence for multiple sources in the Hawaiian plume. *Geochem. Geophys. Geosyst.* **4**. http://dx.doi.org/10.1029/2001GC000271.

Fekiacova Z., Abouchami W., Galer S. J. G., Garcia M. O. and Hofmann A. W. (2007) Origin and temporal evolution of Koolau Volcano, Hawaii: inferences from isotope data on the Koolau Scientific Drilling Project (KSDP), the Honolulu Volcanics and ODP Site 843. *Earth Planet. Sci. Lett.* **261**, 65–83.

Frey F. A., Wise W. S., Garcia M. O., West H., Kwon S. T. and Kennedy A. (1990) Evolution of Mauna-Kea Volcano, Hawaii – petrologic and geochemical constraints on postshield volcanism. *J. Geophys. Res. Solid Earth Planets* **95**, 1271–1300.

Frey F. A., Garcia M. O., Wise W. S., Kennedy A., Gurriet P. and Albarède F. (1991) The evolution of Mauna-Kea Volcano, Hawaii – petrogenesis of tholeiitic and alkalic basalts. *J. Geophys. Res. Solid Earth Planets* **96**, 14347–14375.

Frey F. A., Garcia M. O. and Roden M. F. (1994) Geochemical characteristics of Koolau Volcano – implications of intershield geochemical differences among Hawaiian Volcanos. *Geochim. Cosmochim. Acta* **58**, 1441–1462.

Gaffney A. M., Nelson B. K. and Blichert-Toft J. (2004) Geochemical constraints on the role of oceanic lithosphere in intra-volcano heterogeneity at West Maui, Hawaii. *J. Petrol.* **45**, 1663–1687.

Gaffney A. M., Nelson B. K. and Blichert-Toft J. (2005) Melting in the Hawaiian plume at 1–2 Ma as recorded at Maui Nui: the role of eclogite, peridotite, and source mixing. *Geochem. Geophys. Geosyst.* **6**. http://dx.doi.org/10.1029/2005GC000927.

Galer S. J. G. (1999) Optimal double and triple spiking for high precision lead isotopic measurement. *Chem. Geol.* **157**, 255–274.

Galer S. J. G. and Abouchami W. (1998) Practical application of lead triple spiking for correction of instrumental mass discrimination. *Mineral. Mag.* **62A**, 491–492.

Galer S. J. G. and O'Nions R. K. (1985) Residence time of thorium, uranium and lead in the mantle with implications for mantle convection. *Nature* **316**, 778–782.

Garcia M. O., Pietruszka A. J., Rhodes J. M. and Swanson K. (2000) Magmatic processes during the prolonged Pu'u 'O'o eruption of Kilauea Volcano, Hawaii. *J. Petrol.* **41**, 967–990.

Ghiorso M. S. and Sack R. O. (1995) Chemical mass-transfer in magmatic processes. 4. A revised and internally consistent thermodynamic model for the interpolation and extrapolation of liquid–solid equilibria in magmatic systems at elevated-temperatures and pressures. *Contrib. Mineral. Petrol.* **119**, 197–212.

Hauri E. H. (1996) Major-element variability in the Hawaiian mantle plume. *Nature* **382**, 415–419.

Hauri E. H., Lassiter J. C. and DePaolo D. J. (1996) Osmium isotope systematics of drilled lavas from Mauna Loa, Hawaii. *J. Geophys. Res. Solid Earth* **101**, 11793–11806.

Herzberg C. (2005) Mantle geochemistry: big lessons from little droplets. *Nature* **436**, 789–790.

Herzberg C. (2011) Basalts as temperature probes of Earth's mantle. *Geology* **39**, 1179–1180.

Hofmann A. W. and Farnetani C. G. (2013) Two views of Hawaiian plume structure. *Geochem. Geophys. Geosyst.* **14**, 5308–5322.

Hofmann A. W. and Jochum K. P. (1996) Source characteristics derived from very incompatible trace elements in Mauna Loa and Mauna Kea basalts, Hawaii Scientific Drilling Project. *J. Geophys. Res. Solid Earth* **101**, 11831–11839.

Hofmann A. W. and White W. M. (1983) Ba, Rb and Cs in the Earth's mantle. *Zeitschrift Fur Naturforschung (Section a)* **38**, 256–266.

Hofmann A. W., Jochum K. P., Seufert M. and White W. M. (1986) Nb and Pb in oceanic basalts – new constraints on mantle evolution. *Earth Planet. Sci. Lett.* **79**, 33–45.

Huang S. and Frey F. A. (2003) Trace element abundances of Mauna Kea basalt from phase 2 of the Hawaii Scientific Drilling Project: petrogenetic implications of correlations with major element content and isotopic ratios. *Geochem. Geophys. Geosyst.* **4**. http://dx.doi.org/10.1029/2002GC000322.

Huang S. and Frey F. A. (2005a) The geochemical structure of the Hawaiian plume. *Eos Trans. AGU* **86**(52) (Fall Meet. Suppl. #V51A-1466 (abstr.)).

Huang S. and Frey F. A. (2005b) Recycled oceanic crust in the Hawaiian plume: evidence from temporal geochemical variations within the Koolau Shield. *Contrib. Mineral. Petrol.* **149**, 556–575.

Huang S., Frey F. A., Blichert-Toft J., Fodor R. V., Bauer G. R. and Xu G. (2005) Enriched components in the Hawaiian plume: evidence from Kahoolawe Volcano, Hawaii. *Geochem. Geophys. Geosyst.* **6**. http://dx.doi.org/10.1029/2005GC001012.

Huang S., Abouchami W., Blichert-Toft J., Clague D. A., Cousens B. L., Frey F. A. and Humayun M. (2009) Ancient carbonate sedimentary signature in the Hawaiian plume: evidence from Mahukona Volcano, Hawaii. *Geochem. Geophys. Geosyst.* **10**.

Huang S., Hall P. S. and Jackson M. G. (2011) Geochemical zoning of volcanic chains associated with Pacific hotspots. *Nat. Geosci.* **4**, 874–878.

Huang S., Blichert-Toft J., Fodor R. V., Bauer G. R. and Bizimis M. (2013) Sr, Nd, Hf and Pb isotope systematics of postshield-stage lavas at Kahoolawe, Hawaii. *Chem. Geol.* **360–361**, 159–172.

Ito G. and Mahoney J. J. (2005) Flow and melting of a heterogeneous mantle: 2. Implications for a chemically nonlayered mantle. *Earth Planet. Sci. Lett.* **230**, 47–63.

Jackson E. D., Silver E. A. and Dalrymple G. B. (1972) Hawaiian-Emperor chain and its relation to Cenozoic circumpacific tectonics. *Geol. Soc. Am. Bull.* **83**, 601–618.

Jackson M. C., Frey F. A., Garcia M. O. and Wilmoth R. A. (1999) Geology and geochemistry of basaltic lava flows and dikes from the Trans-Koolau tunnel, Oahu, Hawaii. *Bull. Volcanol.* **60**, 381–401.

Jackson M. G., Hart S. R., Koppers A. A. P., Staudigel H., Konter J., Blusztajn J., Kurz M. and Russell J. A. (2007) The return of subducted continental crust in Samoan lavas. *Nature* **448**, 684–687.

Jackson M. G., Weis D. and Huang S. (2012) Major element variations in Hawaiian shield lavas: source features and perspectives from global ocean island basalt (OIB) systematics. *Geochem. Geophys. Geosyst.* **13**, Q09009.

Jochum K. P. and Hofmann A. W. (1995) *Contrasting Th/U in Historical Mauna Loa and Kilauea Lavas, Mauna Loa Revealed: Structure, Composition, History, and Hazards*. Geophys. Monogr. Ser. AGU, Washington, DC, pp. 307–314.

Kelley K. A., Plank T., Farr L., Ludden J. and Staudigel H. (2005) Subduction cycling of U, Th, and Pb. *Earth Planet. Sci. Lett.* **234**, 369–383.

Kennedy A. K., Kwon S. T., Frey F. A. and West H. B. (1991) The isotopic composition of postshield lavas from Mauna-Kea Volcano, Hawaii. *Earth Planet. Sci. Lett.* **103**, 339–353.

Klein E. M. and Langmuir C. H. (1987) Global correlations of ocean ridge basalt chemistry with axial depth and crustal thickness. *J. Geophys. Res. Solid Earth* **92**, 8089–8115.

Kurz M. D., Kenna T. C., Kammer D. P., Rhodes J. M. and Garcia M. O. (1995) Isotopic evolution of Mauna Loa volcano: a view from the submarine Southwest Rift Zone. In *Mauna Loa Revealed: Structure, Composition, History, and Hazards* (eds. J. M. Rhodes and J. P. Lockwood). Geophysical Monograph, AGU, Washington, D.C., pp. 289–306.

Kurz M. D., Curtice J., Lott D. E. and Solow A. (2004) Rapid helium isotopic variability in Mauna Kea shield lavas from the Hawaiian Scientific Drilling Project. *Geochem. Geophys. Geosyst.* **5**. http://dx.doi.org/10.1029/2002GC000439.

Lassiter J. C., DePaolo D. J. and Tatsumoto M. (1996) Isotopic evolution of Mauna Kea volcano: results from the initial phase of the Hawaii Scientific Drilling Project. *J. Geophys. Res. Solid Earth* **101**, 11769–11780.

Lee C. T. A., Luffi P., Plank T., Dalton H. and Leeman W. P. (2009) Constraints on the depths and temperatures of basaltic magma generation on Earth and other terrestrial planets using new thermobarometers for mafic magmas. *Earth Planet. Sci. Lett.* **279**, 20–33.

Leeman W. P., Gerlach D. C., Garcia M. O. and West H. B. (1994) Geochemical variations in lavas from Kahoolawe Volcano, Hawaii – evidence for open system evolution of plume-derived magmas. *Contrib. Mineral. Petrol.* **116**, 62–77.

Macdonald G. A. (1972) *Volcanoes*. Prentice-Hall Inc., New Jersey, p. 510.

Macdonald G. A. and Katsura T. (1964) Chemical compositional of Hawaiian lavas. *J. Petrol.* **5**, 82–133.

Marske J. P., Pietruszka A. J., Weis D., Garcia M. O. and Rhodes J. M. (2007) Rapid passage of a small-scale mantle heterogeneity through the melting regions of Kilauea and Mauna Loa Volcanoes. *Earth Planet. Sci. Lett.* **259**, 34–50.

Matzen A. K., Baker M. B., Beckett J. R. and Stolper E. M. (2011) Fe–Mg partitioning between olivine and high-magnesian melts and the nature of Hawaiian parental liquids. *J. Petrol.* **52**, 1243–1263.

Mcdonough W. F. and Sun S. S. (1995) The composition of the Earth. *Chem. Geol.* **120**, 223–253.

Moore J. G. and Clague D. A. (1987) Coastal lava flows from Mauna Loa and Hualalai volcanoes, Kona, Hawaii. *Bull. Volcanol.* **49**, 752–764.

Morgan J. P. and Morgan W. J. (1999) Two-stage melting and the geochemical evolution of the mantle: a recipe for mantle plum-pudding. *Earth Planet. Sci. Lett.* **170**, 215–239.

Morgan J. K., Clague D. A., Borchers D. C., Davis A. S. and Milliken K. L. (2007) Mauna Loa's submarine western flank: landsliding, deep volcanic spreading, and hydrothermal alteration. *Geochem. Geophys. Geosyst.* **8**.

Ozawa A., Tagami T. and Garcia M. O. (2005) Unspiked K–Ar dating of the Honolulu rejuvenated and Ko'olau shield

volcanism on O'ahu, Hawai'i. *Earth Planet. Sci. Lett.* **232**, 1–11.

Pietruszka A. J. and Garcia M. O. (1999) The size and shape of Kilauea Volcano's summit magma storage reservoir: a geochemical probe. *Earth Planet. Sci. Lett.* **167**, 311–320.

Pietruszka A. J., Norman M. D., Garcia M. O., Marske J. P. and Burns D. H. (2013) Chemical heterogeneity in the Hawaiian mantle plume from the alteration and dehydration of recycled oceanic crust. *Earth Planet. Sci. Lett.* **361**, 298–309.

Price J. P. and Elliott-Fisk D. (2004) Topographic history of the Maui Nui complex, Hawaii, and its implications for biogeography. *Pacific Sci.* **58**, 27–45.

Putirka K. D. (2008) Thermometers and barometers for volcanic systems. *Rev. Mineral. Geochem.* **69**, 61–120.

Putirka K., Ryerson F. J., Perfit M. and Ridley W. I. (2011) Mineralogy and composition of the oceanic mantle. *J. Petrol.* **52**, 279–313.

Ren Z. Y., Ingle S., Takahashi E., Hirano N. and Hirata T. (2005) The chemical structure of the Hawaiian mantle plume. *Nature* **436**, 837–840.

Ren Z. Y., Shibata T., Yoshikawa M., Johnson K. T. M. and Takahashi E. (2006) Isotope compositions of submarine Hana Ridge lavas, Haleakala volcano, Hawaii: implications for source compositions, melting process and the structure of the Hawaiian plume. *J. Petrol.* **47**, 255–275.

Ren Z.-Y., Hanyu T., Miyazaki T., Chang Q., Kawabata H., Takahashi T., Hirahara Y., Nichols A. R. L. and Tatsumi Y. (2009) Geochemical differences of the Hawaiian Shield Lavas: implications for melting process in the heterogeneous Hawaiian plume. *J. Petrol.* **50**, 1553–1573.

Rhodes J. M. (1995) The 1852 and 1868 Mauna Loa picrite eruptions: clues to parental magma compositions and the magmatic plumbing system. In *Mauna Loa Revealed: Structure, Composition, History, and Hazards* (eds. J. M. Rhodes and J. P. Lockwood). Geophysical Monograph, AGU, Washington, D.C., pp. 241–262.

Rhodes J. M. (1996) Geochemical stratigraphy of lava flows sampled by the Hawaii Scientific Drilling Project. *J. Geophys. Res. Solid Earth* **101**, 11729–11746.

Rhodes J. M. and Hart S. R. (1995) Episodic trace element and isotopic variations in historical Mauna Loa lavas: implications for Magma and plume dynamics. In *Mauna Loa Revealed: Structure, Composition, History, and Hazards* (eds. J. M. Rhodes and J. P. Lockwood). Geophysical Monograph, AGU, Washington, D.C., pp. 263–288.

Rhodes J. M. and Vollinger M. J. (2004) Composition of basaltic lavas sampled by phase-2 of the Hawaii Scientific Drilling Project: geochemical stratigraphy and magma types. *Geochem. Geophys. Geosyst.* **5**. http://dx.doi.org/10.1029/2002GC000434.

Rhodes J. M., Huang S., Frey F. A., Pringle M. and Xu G. (2012) Compositional diversity of Mauna Kea shield lavas recovered by the Hawaii Scientific Drilling Project: inferences on source lithology, magma supply, and the role of multiple volcanoes. *Geochem. Geophys. Geosyst.* **13**, Q03014.

Roden M. F., Trull T., Hart S. R. and Frey F. A. (1994) New He, Nd, Pb, and Sr isotopic constraints on the constitution of the Hawaiian plume – results from Koolau Volcano, Oahu, Hawaii, USA. *Geochim. Cosmochim. Acta* **58**, 1431–1440.

Salters V. J. M. and Stracke A. (2004) Composition of the depleted mantle. *Geochem. Geophys. Geosyst.* **5**, Q05B07.

Salters V. J. M., Blichert-Toft J., Fekiacova Z., Sachi-Kocher A. and Bizimis M. (2006) Isotope and trace element evidence for depleted lithosphere in the source of enriched Ko'olau basalts. *Contrib. Mineral. Petrol.* **151**, 297–312.

Sims K. W. W., DePaolo D. J., Murrell M. T., Baldridge W. S., Goldstein S., Clague D. and Jull M. (1999) Porosity of the melting zone and variations in the solid mantle upwelling rate beneath Hawaii: inferences from U-238–Th-230–Ra-226 and U-235–Pa-231 disequilibria. *Geochim. Cosmochim. Acta* **63**, 4119–4138.

Sleep N. H. (1984) Tapping of magmas from ubiquitous mantle heterogeneities: an alternative to mantle plumes? *J. Geophys. Res. Solid Earth* **89**, 10029–10041.

Sobolev A. V., Hofmann A. W. and Nikogosian I. K. (2000) Recycled oceanic crust observed in 'ghost plagioclase' within the source of Mauna Loa lavas. *Nature* **404**, 986–990.

Sobolev A. V., Hofmann A. W., Sobolev S. V. and Nikogosian I. K. (2005) An olivine-free mantle source of Hawaiian shield basalts. *Nature* **434**, 590–597.

Staudigel H., Davies G. R., Hart S. R., Marchant K. M. and Smith B. M. (1995) Large-scale isotopic Sr, Nd and O isotopic anatomy of altered oceanic-crust – Dsdp/Odp sites-417/418. *Earth Planet. Sci. Lett.* **130**, 169–185.

Stearns H. T. (1946). , p. 106.

Stille P., Unruh D. M. and Tatsumoto M. (1986) Pb, Sr, Nd, and Hf isotopic constraints on the origin of Hawaiian basalts and evidence for a unique mantle source. *Geochim. Cosmochim. Acta* **50**, 2303–2319.

Stolper E., Sherman S., Garcia M., Baker M. and Seaman C. (2004) Glass in the submarine section of the HSDP2 drill core, Hilo, Hawaii. *Geochem. Geophys. Geosyst.* **5**. http://dx.doi.org/10.1029/2003GC000553.

Stracke A., Salters V. J. M. and Sims K. W. W. (1999) Assessing the presence of garnet-pyroxenite in the mantle sources of basalts through combined hafnium–neodymium–thorium isotope systematics. *Geochem. Geophys. Geosyst.* **1**. http://dx.doi.org/10.1029/1999GC000013.

Takahashi E. and Nakajima K. (2002) *Melting Process in the Hawaiian Plume: An Experimental Study, Hawaiian Volcanoes: Deep Underwater Perspectives*. Geophys. Monogr. Ser. AGU, Washington, DC, pp. 403–418.

Tanaka R., Nakamura E. and Takahashi E. (2002) Geochemical evolution of Koolau Volcano, Hawaii. In *Hawaiian Volcanoes: Deep Underwater Perspectives. Geophysical Monograph Series* (eds. E. Takahashi, P. Leeman, M. Garcia, J. Naka and S. Aramaki). Geophysical Monograph, AGU, Washington, D.C., pp. 311–332.

Tanaka R., Makishima A. and Nakamura E. (2008) Hawaiian double volcanic chain triggered by an episodic involvement of recycled material: constraints from temporal Sr–Nd–Hf–Pb isotopic trend of the Loa-type volcanoes. *Earth Planet. Sci. Lett.* **265**, 450–465.

Tatsumoto M. (1978) Isotopic composition of lead in oceanic basalt and its implication to mantle evolution. *Earth Planet. Sci. Lett.* **38**, 63–87.

Wanless V. D., Garcia M. O., Trusdell F. A., Rhodes J. M., Norman M. D., Weis D., Fornari D. J., Kurz M. D. and Guillou H. (2006) Submarine radial vents on Mauna Loa Volcano, Hawai'i. *Geochem. Geophys. Geosyst.* **7**.

Weis D., Garcia M. O., Rhodes J. M., Jellinek M. and Scoates J. S. (2011) Role of the deep mantle in generating the compositional asymmetry of the Hawaiian mantle plume. *Nature Geosci.* **4**, 831–838.

West H. B., Gerlach D. C., Leeman W. P. and Garcia M. O. (1987) Isotopic constraints on the origin of Hawaiian lavas from the Maui Volcanic complex, Hawaii. *Nature* **330**, 216–220.

Workman R. K., Hart S. R., Jackson M., Regelous M., Farley K. A., Blusztajn J., Kurz M. and Staudigel H. (2004) Recycled metasomatized lithosphere as the origin of the enriched mantle II (EM2) end-member: evidence from the Samoan volcanic chain. *Geochem. Geophys. Geosyst.* **5**. http://dx.doi.org/10.1029/2003GC000623.

Wright T. L. and Fiske R. S. (1971) Origin of differentiated and hybrid lavas of Kilauea Volcano, Hawaii. *J. Petrol.* **12**, 1–65.

Xu G., Frey F. A., Clague D. A., Weis D. and Beeson M. H. (2005) East Molokai and other Kea-trend volcanoes: magmatic processes and sources as they migrate away from the Hawaiian hot spot. *Geochem. Geophys. Geosyst.* **6**. http://dx.doi.org/10.1029/2004GC000830.

Xu G., Frey F., Clague D., Abouchami W., BlichertToft J. and Cousens B. L. (2007) Geochemical characteristics of West Molokai shield- and postshield-stage lavas: constraints on Hawaiian plume models. *Geochem. Geophys. Geosyst.* **8**. http://dx.doi.org/10.1029/2006GC001554.

Yamasaki S., Kani T., Hanan B. B. and Tagami T. (2009) Isotopic geochemistry of Hualalai shield-stage tholeiitic basalts from submarine North Kona region, Hawaii. *J. Volcanol. Geoth. Res.* **185**, 223–230.

Yang H. J., Frey F. A. and Clague D. A. (2003) Constraints on the source components of lavas forming the Hawaiian north arch and Honolulu Volcanics. *J. Petrol.* **44**, 603–627.

Associate editor: Marc Norman

Supplementary material

The Distribution of Geochemical Heterogeneities in the Source of Hawaiian Shield Lavas as Revealed by a Transect Across the Strike of the Loa and Kea Spatial Trends: East Molokai to West Molokai to Penguin Bank

by Xu et al.

Table S1. Sample locations and water depth for Pisces V dive samples

Sample #	Water depth	Sampling notes
P5-255-1	1815 m	5 small pieces, 1”-2.5” across, from Mn-encrusted pillow outcrop
P5-255-2	1800 m	from shattered pillow outcrop
P5-255-3	1760 m	knobby lava fragment from pillow breccia unit
P5-255-4	1710 m	white carbonate cementing pillow fragments
P5-255-5	1710 m	pillow wedge in debris chute
P5-255-6	1660 m	fragmental basalt in cemented debris chute
P5-255-7	1620 m	rounded basalt fragment from pillow outcrop
P5-255-8	1565 m	knobby basalt fragment
P5-255-9	1550 m	from breccia outcrop
P5-255-10	1465 m	probable pillow lava
P5-255-11	1400 m	pillow lava from step cliff
P5-255-12	1320 m	small lava fragment from breccia
P5-255-13	1320 m	small lava fragment from breccia
P5-255-14	1250 m	rounded knobby basalt
P5-255-15	1250 m	probably from dike
P5-255-16	1210 m	lava sample from dense flow

Table S2. Compositions of glass and coexisting olivine and compositions of glass inclusions in olivine

Sample	SiO2	TiO2	Al2O3	FeO	MnO	MgO	CaO	Na2O	K2O	P2O5	NiO	Cr2O3	S	Cl	Total	Fo%
Glass composition																
Penguin Bank Deep Rift																
MV-D10-R2	51.70	2.68	13.49	11.70	0.16	5.96	10.31	2.46	0.52	0.31			0.009	0.009	99.42	
MV-D10-R3	52.09	2.80	13.56	11.67	0.18	5.87	10.26	2.47	0.52	0.31			0.008	0.006	99.88	
MV-D10-R4	51.88	2.94	13.45	11.59	0.17	5.73	10.17	2.53	0.58	0.34			0.010	0.007	99.51	
MV-D10-R4 relicate	51.86	2.97	13.47	11.57	0.16	5.79	10.14	2.61	0.59	0.37			0.010	0.013	99.54	
MV-D10-R5	51.91	2.79	13.45	11.60	0.17	5.90	10.33	2.53	0.52	0.31			0.015	0.006	99.64	
MV-D10-R5 replicate	51.70	2.75	13.49	11.67	0.18	5.99	10.35	2.43	0.50	0.32			0.013	0.012	99.43	
MV-D11-R1 #3	50.97	2.29	13.39	11.54	0.20	7.68	10.92	2.13	0.37	0.19			0.046	0.001	99.72	
MV-D11-R1 #4	51.08	2.36	13.46	11.35	0.12	7.69	10.98	2.17	0.38	0.21			0.055	0.002	99.85	
MV-D11-R1 #5	50.47	2.12	12.47	10.96	0.20	10.05	10.24	2.00	0.33	0.17			0.034	0.000	99.03	
MV-D11-R1 #6	51.51	2.35	13.73	11.09	0.16	7.43	10.95	2.16	0.32	0.24			0.034	0.005	99.99	
MV-D11-R1 #9	51.20	2.36	13.51	11.21	0.17	7.62	10.93	2.09	0.37	0.18			0.044	0.007	99.70	
MV-D11-R1 #13	51.70	2.18	13.67	10.51	0.10	7.50	10.59	2.18	0.31	0.18			0.068	0.000	98.98	
MV-D11-R1 #15	51.55	2.53	13.51	11.45	0.18	7.95	10.60	1.83	0.38	0.22			0.073	0.004	100.27	
MV-D11-R1 #16	50.89	2.35	13.22	11.32	0.21	8.13	10.86	2.11	0.36	0.20			0.036	0.006	99.69	
MV-D11-R1 #17	51.30	2.22	13.03	11.12	0.18	8.45	10.54	2.04	0.35	0.22			0.088	0.019	99.56	
MV-D11-R1 #18	51.25	2.39	13.10	11.32	0.18	8.52	10.44	2.13	0.34	0.24			0.048	0.000	99.94	
MV-D11-R1 #19	51.62	2.29	13.56	10.98	0.18	7.51	10.64	2.23	0.37	0.21			0.077	0.000	99.66	
MV-D11-R1 #20	50.89	2.40	13.47	11.25	0.22	7.82	10.91	2.13	0.36	0.21			0.048	0.007	99.71	
Pisces V dive																
P5-255-3-1	52.36	2.99	13.37	12.06	0.17	5.58	9.79	2.48	0.66	0.39			0.021	0.011	99.88	
P5-255-3-4	52.07	2.91	13.24	12.51	0.17	5.54	9.81	2.45	0.65	0.4			0.009	0.004	99.76	
P5-255-3-5	52	2.95	13.12	12.41	0.17	5.54	9.85	2.46	0.64	0.39			0.007	0.006	99.54	
P5-255-3-6	52	3.01	13.21	12.38	0.15	5.57	9.88	2.48	0.64	0.38			0.006	0.014	99.72	
P5-255-3-7	51.82	2.89	13.12	12.26	0.17	5.42	9.88	2.45	0.63	0.39			0.007	0.01	99.05	
P5-255-3-8	51.91	2.97	12.93	12.6	0.17	6.25	9.52	2.4	0.66	0.38			0.007	0.007	99.80	
P5-255-3A-1	52.1	3.14	13.28	12.26	0.17	4.91	10.07	2.15	0.65	0.39			0.02	0.011	99.15	
P5-255-3A-2	51.81	3.01	13.18	12.33	0.18	5.37	9.84	2.27	0.65	0.37			0.031	0.012	99.05	
P5-255-3A-3	51.88	2.93	13.16	12.28	0.18	5.46	9.85	2.43	0.64	0.40			0.014	0.009	99.23	
P5-255-3A-6	51.13	3.19	12.77	12.72	0.18	5.26	9.57	2.18	0.7	0.40			0.007	0.01	98.12	
P5-255-3A-7	51.63	2.97	13.1	12.41	0.18	5.49	9.88	2.36	0.64	0.39			0.008	0.012	99.07	
P5-255-7-5	51.84	3.51	12.76	12.96	0.17	5	9.34	2.33	0.74	0.46			0.009	0.012	99.13	
P5-255-7-6	52.3	3.55	13.33	11.68	0.17	5.18	9.55	2.32	0.74	0.47			0.012	0.009	99.31	
P5-255-7-10	51.83	3.70	12.67	13.49	0.18	4.87	9.32	2.09	0.72	0.47			0.006	0.011	99.36	
P5-255-7-11	52.16	3.48	13.08	12.32	0.17	5.19	9.39	2.25	0.73	0.48			0.011	0.014	99.28	
P5-255-7-12	51.93	3.55	12.95	12.33	0.18	5.26	9.43	2.46	0.73	0.5			0.019	0.01	99.35	
P5-255-8-3	51.86	3.43	13.14	12.81	0.19	4.72	9.52	2.22	0.72	0.45			0.007	0.016	99.08	
P5-255-8-4	51.94	3.48	13.07	12.64	0.19	4.75	9.47	2.25	0.72	0.46			0.01	0.011	98.99	
P5-255-8-5	52.13	3.46	13.08	12.47	0.18	4.96	9.6	2.22	0.75	0.46			0.008	0.01	99.33	
P5-255-8-6	51.91	3.66	12.86	13.09	0.18	4.72	9.38	2.1	0.69	0.50			0.012	0.02	99.12	

P5-255-8-7	51.94	3.58	12.86	13.06	0.18	4.78	9.4	2.28	0.78	0.48	0.006	0.012	99.36
P5-255-8-8	52.24	2.96	14.25	11.34	0.17	4.91	10.19	2.59	0.75	0.38	0.03	0.004	99.81
P5-255-12A-1	50.75	3.24	13.2	12.44	0.18	5.6	10.12	2.66	0.66	0.42	0.008	0.014	99.29
P5-255-12A-2	50.89	3.23	13.24	12.54	0.19	5.53	10.14	2.63	0.67	0.43	0.01	0.009	99.51
P5-255-12A-4	50.39	3.18	13.41	12.28	0.17	5.53	10.22	2.64	0.65	0.42	0.008	0.012	98.91
P5-255-12A-6	50.47	3.35	13.17	12.42	0.18	5.54	10.11	2.7	0.64	0.42	0.01	0.011	99.02
P5-255-12A-7	50.75	3.26	13.12	12.36	0.16	5.64	10.11	2.6	0.66	0.41	0.009	0.015	99.09
P5-255-12A-8	50.71	3.21	13.19	12.12	0.18	5.67	10.2	2.67	0.67	0.41	0.025	0.015	99.07
P5-255-12A-9	50.72	3.18	13.22	12.24	0.18	5.66	10.17	2.65	0.67	0.43	0.017	0.015	99.15
P5-255-12A-10	50.66	3.26	13.21	12.32	0.17	5.66	10.13	2.62	0.65	0.44	0.007	0.015	99.14
P5-255-12A-11	50.5	3.27	13.15	12.53	0.17	5.62	10.16	2.67	0.65	0.42	0.009	0.01	99.16
P5-255-12A-12	50.65	3.37	13.06	12.64	0.17	5.49	10.04	2.69	0.67	0.44	0.009	0.012	99.24
P5-255-12A-13	51.05	3.31	13.23	12.53	0.19	5.49	10.05	2.6	0.67	0.44	0.007	0.011	99.58
P5-255-12A-14	50.64	3.29	13.19	12.25	0.19	5.56	10.15	2.74	0.66	0.43	0.006	0.011	99.12
P5-255-12A-15	50.75	3.22	13.41	12.47	0.19	5.54	10.09	2.7	0.66	0.43	0.011	0.011	99.48
P5-255-12B-1	50.84	3.24	13.31	12.32	0.17	5.65	10.2	2.62	0.66	0.42	0.008	0.009	99.45
P5-255-12B-2	50.56	3.2	13.2	12.44	0.19	5.78	10.36	2.62	0.65	0.41	0.011	0.011	99.43
P5-255-12B-3	51.05	3.16	13.14	12.36	0.17	5.78	10.34	2.67	0.64	0.42	0.01	0.015	99.76
P5-255-12B-4	50.82	3.42	13.05	12.93	0.19	5.36	9.77	2.61	0.65	0.45	0.004	0.01	99.26
P5-255-12B-5	51.03	3.45	13.06	13.05	0.16	5.3	9.77	2.61	0.72	0.46	0.011	0.01	99.63
P5-255-12B-6	50.93	3.32	13.02	13.09	0.18	5.35	9.88	2.65	0.67	0.46	0.003	0.011	99.56
P5-255-12B-7	50.68	3.3	13.22	12.58	0.17	5.52	10.03	2.64	0.69	0.43	0.008	0.011	99.28
P5-255-12B-8	50.51	3.27	13.04	12.54	0.17	5.47	10.03	2.67	0.64	0.44	0.008	0.013	98.80
P5-255-12B-9	50.5	3.33	13.03	12.54	0.19	5.41	9.96	2.73	0.66	0.45	0.009	0.016	98.83
P5-255-12B-10	50.63	3.39	13.1	12.82	0.18	5.48	9.9	2.68	0.67	0.44	0.009	0.01	99.31
P5-255-12B-11	50.72	3.41	13.12	13.42	0.19	4.97	9.66	2.43	0.73	0.47	0.004	0.016	99.14
P5-255-12B-12	50.69	3.43	13	12.98	0.18	5.25	9.82	2.64	0.7	0.46	0.003	0.01	99.16
P5-255-12B-13	50.8	3.48	12.97	12.87	0.18	5.3	9.82	2.66	0.7	0.45	0.007	0.013	99.25
P5-255-12B-14	51.08	3.5	13.07	12.97	0.19	5.37	9.79	2.66	0.71	0.46	0.006	0.014	99.82
P5-255-12B-15	52.18	2.96	13.27	12.56	0.17	5.43	9.96	2.51	0.63	0.39	0.009	0.007	100.08
P5-255-13A-2	52.04	2.98	13.29	12.55	0.19	5.4	9.94	2.48	0.65	0.4	0.01	0.01	99.94
P5-255-13A-3	51.95	2.93	13.22	12.8	0.16	5.38	9.96	2.49	0.64	0.39	0.007	0.01	99.94
P5-255-13A-4	52.07	2.99	13.14	12.34	0.17	5.67	9.93	2.48	0.67	0.4	0.008	0.007	99.88
P5-255-13A-5	51.89	2.9	12.78	12.28	0.18	6.27	10.33	2.32	0.61	0.37	0.005	0.008	99.94
P5-255-13A-6	52.21	2.96	13.25	12.29	0.18	5.56	10.03	2.53	0.65	0.39	0.007	0.01	100.07
P5-255-13A-7	52.06	2.93	13.31	12.26	0.18	5.53	10	2.55	0.64	0.4	0.008	0.008	99.88
P5-255-13A-8	51.75	2.97	13.18	12.42	0.17	5.53	10.03	2.52	0.63	0.38	0.008	0.008	99.60
P5-255-13A-9	52.66	3.07	13.82	11.68	0.16	5.22	9.72	1.76	0.68	0.4	0.016	0.011	99.20
P5-255-13A-10	51.94	3.05	13.37	12.59	0.17	5.45	9.77	1.93	0.64	0.41	0.005	0.011	99.34
P5-255-16-3	52.07	3.02	13.31	12.4	0.16	5.48	9.83	1.96	0.64	0.41	0.008	0.009	99.30
P5-255-16-4	51.12	3.28	13.37	12.43	0.18	5.58	10.24	2.65	0.65	0.42	0.005	0.004	99.93
P5-255-16-5	51.04	3.22	13.33	12.48	0.18	5.56	10.26	2.63	0.67	0.43	0.009	0.011	99.82
P5-255-MUD-1	51.02	3.2	13.39	12.32	0.18	5.7	10.26	2.68	0.66	0.42	0.007	0.011	99.85
P5-255-MUD-2	52.05	3.34	13.46	12.27	0.16	5.03	9.88	2.57	0.67	0.43	0.001	0.012	99.87

P5-255-MUD-3	51.16	3.3	13.37	12.57	0.16	5.53	10.25	2.62	0.66	0.43	0.01	0.014	100.07
P5-255-MUD-4	51.23	3.33	13.41	12.51	0.17	5.55	10.26	2.72	0.65	0.43	0.008	0.012	100.28
P5-255-MUD-5	52.09	3.05	13.42	11.72	0.16	5.46	10.07	2.45	0.63	0.4	0.005	0.011	99.47
P5-255-MUD-6	50.88	3.18	13.33	12.09	0.14	5.61	10.33	2.7	0.64	0.41	0.01	0.013	99.33
P5-255-MUD-7	51.06	3.3	13.21	12.64	0.16	5.47	10.14	2.68	0.66	0.44	0.008	0.012	99.78
P5-255-MUD-8	51.01	3.28	13.35	12.5	0.18	5.56	10.22	2.73	0.65	0.42	0.011	0.013	99.92
P5-255-MUD-9	51.08	3.57	12.95	13.2	0.2	5.26	9.8	2.74	0.73	0.48	0.002	0.007	100.02
P5-255-MUD-10	51.02	3.36	13.07	12.86	0.17	5.32	9.93	2.73	0.69	0.44	0.006	0.009	99.61
P5-255-MUD-11	51.92	3.29	13.15	12.34	0.19	5.33	9.75	2.6	0.67	0.44	0.002	0.009	99.69
P5-255-MUD-12	51.98	3.27	13.22	12.18	0.17	5.41	9.8	2.66	0.68	0.42	0.008	0.006	99.80
P5-255-MUD-13	51.01	3.17	13.45	12.2	0.18	5.66	10.35	2.67	0.63	0.41	0.012	0.012	99.75
P5-255-MUD-14	51.06	3.21	13.33	12.44	0.17	5.62	10.23	2.75	0.65	0.42	0.005	0.01	99.90
P5-255-MUD-15	51.07	3.36	13.22	12.4	0.16	5.45	9.99	2.92	0.67	0.43	0.008	0.013	99.69
P5-255-MUD-16	51.12	3.22	13.18	12.26	0.18	5.47	10.17	2.72	0.67	0.43	0.01	0.014	99.44
P5-255-MUD-17	51.23	3.23	13.42	12.46	0.17	5.45	10.26	2.71	0.65	0.43	0.012	0.013	100.04
P5-255-MUD-18	51.07	3.2	13.37	12.22	0.17	5.65	10.25	2.68	0.63	0.43	0.008	0.009	99.69
P5-255-MUD-19	51	3.25	13.27	12.23	0.17	5.56	10.25	2.71	0.65	0.43	0.012	0.013	99.55
P5-255-MUD-20	51.56	3.25	13.07	12.67	0.17	5.45	10.06	2.43	0.61	0.37	0.012	0.009	99.66
P5-255-MUD-21	51.78	3.03	13.25	12.45	0.17	5.35	9.81	2.46	0.65	0.41	0.008	0.01	99.38
P5-255-A-5	51.84	3.01	13.24	12.7	0.17	5.39	9.94	2.52	0.63	0.39	0.008	0.011	99.85
P5-255-A-6	52	3.02	13.23	12.41	0.18	5.39	9.9	2.54	0.65	0.40	0.008	0.009	99.74
P5-255-A-10	52.28	3.03	13.34	12.16	0.16	5.4	9.97	2.51	0.65	0.38	0.014	0.012	99.91
P5-255-A-11	51.88	3.02	13.26	12.6	0.16	5.3	9.8	2.45	0.64	0.40	0.009	0.008	99.53
P5-255-A-13	51.15	3.27	13.3	12.68	0.17	5.33	10.05	2.49	0.67	0.44	0.008	0.013	99.57
P5-255-A-14	51.13	3.25	13.37	12.35	0.17	5.42	10.18	2.71	0.67	0.41	0.01	0.012	99.68
P5-255-B-1	50.95	3.23	13.21	12.5	0.16	5.47	10.16	2.69	0.66	0.41	0.007	0.01	99.46
P5-255-B-3	51.18	3.25	13.37	12.41	0.17	5.52	10.21	2.76	0.67	0.42	0.008	0.012	99.98
P5-255-B-4	50.95	3.26	13.24	12.42	0.17	5.48	10.11	2.64	0.65	0.44	0.01	0.008	99.38
P5-255-B-5	51.11	3.18	13.27	12.24	0.18	5.57	10.23	2.69	0.65	0.43	0.007	0.013	99.57
P5-255-B-6	51.1	3.22	13.24	12.3	0.16	5.54	10.17	2.74	0.68	0.44	0.011	0.009	99.61
P5-255-B-9	51.07	3.29	13.23	12.33	0.16	5.5	10.14	2.71	0.68	0.44	0.009	0.005	99.56
P5-255-B-10	51.12	3.19	13.42	12.44	0.17	5.47	10.18	2.66	0.65	0.43	0.006	0.007	99.74
P5-255-B-11	52.31	3.07	14.3	11.98	0.17	4.97	10.13	2.21	0.66	0.41	0.024	0.01	100.24
P5-255-B-12	51.1	3.23	13.3	12.36	0.16	5.5	10.17	2.7	0.67	0.43	0.009	0.007	99.64
P5-255-C-1	52.42	3.01	13.73	11.79	0.16	5.48	10.11	1.96	0.64	0.41	0.015	0.01	99.74
P5-255-C-2	52.46	2.89	14.5	10.8	0.15	5.56	10.3	2.06	0.62	0.36	0.018	0.01	99.73
P5-255-C-3	52.31	3.21	13.54	12.21	0.17	5.24	9.91	1.91	0.67	0.42	0.007	0.01	99.61
P5-255-C-7	51.14	3.19	13.53	12.4	0.18	5.61	10.34	2.17	0.67	0.42	0.008	0.01	99.67
P5-255-C-8	51.4	3.22	13.56	12.38	0.18	5.6	10.31	2.13	0.66	0.43	0.01	0.01	99.89
P5-255-D-1	51.1	3.23	13.55	12.28	0.16	5.66	10.39	2.16	0.66	0.43	0.009	0.01	99.64
P5-255-D-2	51.3	3.21	13.6	12.4	0.18	5.56	10.26	2.13	0.64	0.43	0.007	0.01	99.73
P5-255-D-3	51.68	3.25	13.94	12.38	0.17	5.73	10.42	2.2	0.64	0.41	0.013	0.01	100.84
P5-255-D-4	50.83	3.19	13.44	12.46	0.18	5.46	9.97	2.83	0.68	0.4	0.008	0.021	99.47
P5-255-D-5	51.01	3.19	13.42	12.22	0.17	5.59	10.31	2.69	0.65	0.42	0.007	0.011	99.69

P5-255-D-6	51.38	3.22	13.5	12.24	0.17	5.62	10.29	2.62	0.67	0.43		0.007	0.008	100.16
P5-255-D-8	52.77	2.96	13.34	11.97	0.15	5.57	9.88	2.38	0.65	0.4		0.008	0.015	100.09
P5-255-G-2	52.29	2.95	13.37	12.31	0.17	5.49	9.98	2.51	0.64	0.39		0.009	0.01	100.12
P5-255-G-7	52.66	2.93	13.47	12.24	0.19	5.45	9.88	2.58	0.61	0.39		0.005	0.01	100.42
P5-255-G-8	52.28	2.97	13.27	12.29	0.16	5.5	9.99	2.51	0.63	0.38		0.011	0.007	100.00
P5-255-G-13	52.35	2.93	13.4	12.27	0.19	5.56	10	2.51	0.62	0.38		0.01	0.009	100.23
P5-255-G-14	52.07	2.95	13.27	12.41	0.17	5.49	9.9	2.4	0.64	0.37		0.007	0.009	99.69
P5-255-H-5	52.54	3.3	13.53	12.5	0.17	4.64	9.66	2.46	0.74	0.32		0.009	0.008	99.88
P5-255-H-7	51.87	3.58	12.92	12.5	0.18	4.25	9.58	2.23	0.75	0.34		0.023	0.01	98.23
P5-255-H-8	52.1	3.54	13.02	13.05	0.15	4.6	9.31	2.39	0.8	0.36		0.008	0.024	99.35
P5-255-H-9	52.41	3.88	12.7	13.41	0.14	4.46	8.95	2.24	0.84	0.39		0.006	0.013	99.44
P5-255-H-10	52.53	3.32	13.09	12.65	0.17	4.65	9.66	2.56	0.76	0.32		0.014	0.008	99.73
P5-255-H-11	52.55	3.46	13.14	12.15	0.16	5.01	9.6	2.4	0.73	0.36		0.013	0.009	99.58
P5-255-H-12	52.4	3.57	13.07	12.71	0.16	4.92	9.48	2.24	0.74	0.35		0.008	0.012	99.66
Glass inclusions in olivine														
P5-255-1-1	53.57	2.37	16.51	8.08	0.12	3.8	12.23	2.29	0.51	0.56		0.118	0.006	100.34
P5-255-1-2	52.44	2.67	14.87	9.82	0.15	4.61	11.76	2.42	0.54	0.34		0.086	0.013	99.85
P5-255-1-3	54.9	1.84	16.02	7.4	0.13	4.14	11.78	2.88	0.46	0.31		0.069	0.008	100.04
P5-255-3-2	52.01	3.04	13.39	12.23	0.17	5.03	10.08	2.48	0.63	0.39		0.008	0.011	99.49
P5-255-3-3	52.11	2.95	13.24	12.31	0.17	5.31	10.02	2.49	0.65	0.39		0.009	0.01	99.66
P5-255-3-4	52.33	2.57	14.95	7.71	0.12	5.96	11.79	2.55	0.51	0.33		0.072	0.008	98.98
P5-255-6A-3	52.29	2.89	15.49	7.86	0.12	5.83	12.06	2.78	0.63	0.38		0.073	0.015	100.52
P5-255-6A-6	52.1	2.44	14.99	8.84	0.11	6.19	12.13	2.42	0.43	0.31		0.101	0.008	100.22
P5-255-6A-7	51.93	2.35	14.99	8.9	0.12	6.19	12.25	2.4	0.44	0.34		0.112	0.014	100.19
P5-255-6A-8	52.09	3.53	13.77	12.35	0.17	4.38	10.55	2.4	0.69	0.43		0.01	0.013	10.41
P5-255-6A-9	51.19	2.61	15.64	8.69	0.13	4.29	14.18	2.29	0.51	0.41		0.058	0.008	10.09
P5-255-7-3	51.52	2.73	14.41	11.17	0.18	5.35	10.52	2.57	0.59	0.36		0.094	0.008	99.64
P5-255-7-4	51.47	2.72	16.01	9.44	0.12	5.06	9.53	2.71	0.64	0.35		0.131	0.032	98.40
P5-255-7-7	53.2	2.26	15.92	8.86	0.13	5.31	9.58	2.92	0.57	0.34		0.078	0.006	99.29
P5-255-7-8	53.49	2.71	15.49	6.23	0.11	5.81	11.73	2.6	0.58	0.36		0.066	0.01	99.28
P5-255-7-9	52.32	2.72	15.56	7.4	0.11	5.75	11.97	2.57	0.45	0.34		0.065	0.012	99.36
P5-255-8-1	52.03	2.56	14.8	9.49	0.14	5.67	11.11	2.52	0.53	0.32		0.096	0.008	99.40
P5-255-8-2	52.15	2.61	15.18	9.21	0.15	5.47	11.35	2.62	0.52	0.33		0.094	0.011	99.82
P5-255-8-11	52.84	2.72	15.4	6.77	0.1	5.77	11.86	2.42	0.63	0.52		0.083	0.011	99.25
P5-255-8-12	53.87	2.43	15.35	7.4	0.11	5.29	12.07	2.37	0.46	0.27		0.07	0.001	99.78
P5-255-8-14	53.96	2.71	15.44	6.12	0.09	5.56	11.83	2.61	0.46	0.27		0.087	0.012	99.26
P5-255-8-15	53.84	2.88	15.78	5.91	0.09	5.25	12.24	2.47	0.49	0.37		0.067	0.011	99.51
P5-255-12B-2A	52	2.41	15.49	8.13	0.12	6.24	12.28	2.69	0.19	0.12		0.023	0.004	99.74
P5-255-13A-1	52.15	2.5	14.7	8.83	0.13	6.13	11.88	2.5	0.36	0.34		0.096	0.009	99.77
P5-255-13A-6	52.65	2.85	13.62	11.08	0.16	5.65	10.42	2.55	0.61	0.36		0.027	0.01	100.03
P5-255-13A-6a	52.46	2.67	14.35	10.5	0.17	5.64	10.55	2.6	0.61	0.33		0.012	0.008	99.90
P5-255-14A-6A	53.86	2.67	15.3	9.08	0.15	4.85	9.45	1.64	0.63	0.44		0.164	0.011	98.48
P5-255-14A-9	51.51	4.01	12.54	15.67	0.2	4.04	8.52	1.56	0.73	0.56		0.002	0.018	99.35

P5-255-16-1	52.48	2.48	14.4	8.28	0.13	6.02	12.46	1.96	0.51	0.32			0.103	0.008	99.31	
P5-255-16-2	52.38	3.04	13.43	12.14	0.17	5.44	9.81	1.85	0.67	0.42			0.009	0.012	99.37	
P5-255-16-7	52.18	2.96	13.42	12.22	0.17	5.31	9.82	1.87	0.64	0.4			0.017	0.008	99.05	
P5-255-16-9	52.14	1.46	13.03	8.79	0.14	6.48	14.91	1.87	0.26	0.16			0.087	0.002	99.46	
P5-255-16-10	52.67	2.63	16.47	7.62	0.12	5.51	10.46	2.12	0.6	0.46			0.059	0.008	98.81	
P5-255-A-1	53.05	2.26	14.64	8.36	0.12	6.04	11.79	2.53	0.44	0.29			0.106	0.008	99.78	
P5-255-A-3	52.13	2.09	15.21	9.03	0.12	5.9	12.55	2.18	0.4	0.24			0.098	0.011	100.12	
P5-255-A-4	52.03	2.06	15.17	8.79	0.13	6.01	12.54	2.27	0.4	0.26			0.092	0.008	99.90	
P5-255-A-7	51.67	2.54	14.43	10.76	0.15	5.75	10.98	2.48	0.54	0.32			0.1	0.005	99.86	
P5-255-A-7A	52	2.92	13.35	12.1	0.15	5.47	10.19	2.47	0.63	0.38			0.01	0.011	99.77	
P5-255-A-8	52.27	2.44	14.68	9.68	0.14	5.81	11.01	2.57	0.54	0.31			0.115	0.01	99.74	
P5-255-A-9	52.01	2.88	13.32	11.95	0.18	5.42	10.22	2.44	0.64	0.37			0.035	0.011	99.52	
P5-255-A-12	51.94	2	15.2	10.07	0.17	5.98	11.39	2.23	0.45	0.28			0.107	0.005	99.97	
P5-255-B-7	50.75	3.26	13.4	12.49	0.17	5.59	10.14	2.71	0.66	0.42			0.022	0.011	99.65	
P5-255-C-4	52.78	3.01	14.11	11.42	0.16	5.37	10.2	2.04	0.64	0.41			0.012	0.01	100.16	
P5-255-C-5	50.67	2.72	14.38	10.36	0.14	6.02	10.51	2.16	0.56	0.34			0.107	0.01	98.13	
P5-255-C-6	52.41	3.06	13.85	11.7	0.17	5.52	10.24	1.99	0.66	0.39			0.025	0.01	100.07	
P5-255-C-9	53.1	2.6	16.12	8.64	0.12	5.5	10.42	2.14	0.59	0.35			0.069	0.01	99.74	
P5-255-C-10	52.26	3.12	13.51	11.92	0.15	5.36	10.06	1.96	0.64	0.42			0.031	0.01	99.50	
P5-255-D-9	53.45	2.11	15.33	9.01	0.14	5.9	10.46	2.66	0.53	0.36			0.079	0.013	100.16	
P5-255-D-10	51.2	2	13.53	9.52	0.13	6.33	14.47	2.18	0.41	0.25			0.089	0.008	100.27	
P5-255-G-1	53.34	3.19	13.6	11.39	0.16	5.47	9.72	2.46	0.71	0.41			0.012	0.013	100.50	
P5-255-G-5	53.03	2.27	14.85	8.66	0.12	6.08	11.71	2.48	0.43	0.28			0.117	0.007	100.23	
P5-255-G-9	52.81	2.26	12.92	7.88	0.13	6.61	14.53	2.23	0.45	0.36			0.09	0.007	100.41	
P5-255-G-11	52.79	2.87	13.49	11.77	0.18	5.53	9.94	2.55	0.68	0.37			0.027	0.009	100.22	
P5-255-G-12	51.8	2.11	15.55	8.14	0.13	6.27	13.01	2.19	0.52	0.33			0.131	0.006	100.39	
P5-255-H-1	52.26	3.08	12.9	11.11	0.18	5.44	10.78	2.48	0.64	0.28			0.082	0.012	99.37	
P5-255-H-2	52.31	2.58	14.79	9.99	0.15	5.13	10.76	2.71	0.53	0.25			0.073	0.024	99.41	
P5-255-H-6	52.39	3.44	13.05	12.2	0.16	4.77	9.6	2.17	0.76	0.33			0.015	0.018	98.92	
Composition of olivine coexisting with glass																
P5-255-1 1	40.19			14.83	0.18	45.44	0.24				0.30	0.03			101.20	84.5
P5-255-1 2	40.46			11.75	0.16	47.78	0.22				0.35	0.10			100.81	87.9
P5-255-1 3	40.73			11.28	0.15	48.24	0.22				0.43	0.09			101.14	88.4
P5-255-1 4	40.13			15.22	0.18	44.91	0.23				0.45	0.08			101.19	84.0
P5-255-1 5	39.75			15.32	0.21	44.99	0.22				0.42	0.07			100.98	84.0
P5-255-1 6	39.75			15.93	0.19	44.60	0.22				0.37	0.05			101.10	83.3
P5-255-1 7	40.91			10.72	0.16	48.85	0.20				0.45	0.10			101.41	89.0
P5-255-1 8	41.01			11.41	0.17	48.00	0.20				0.45	0.10			101.34	88.2
P5-255-1 9	40.53			12.59	0.17	47.21	0.22				0.42	0.08			101.22	87.0
P5-255-1 10	39.84			16.61	0.22	44.14	0.27				0.30	0.04			101.41	82.6
P5-255-1 11	40.17			14.36	0.21	45.67	0.27				0.29	0.06			101.01	85.0
P5-255-1 12	40.67			11.66	0.15	48.03	0.22				0.39	0.09			101.21	88.0
P5-255-1 13	40.41			11.97	0.17	47.76	0.21				0.38	0.12			101.02	87.7

P5-255-1 14	40.31	14.34	0.18	45.63	0.30	0.36	0.06	101.18	85.0
P5-255-1 15	39.82	16.17	0.22	44.42	0.26	0.29	0.06	101.23	83.0
P5-255-13A 1	40.65	12.41	0.18	47.35	0.23	0.42	0.08	101.32	87.2
P5-255-13A 2	40.68	11.23	0.16	48.00	0.21	0.32	0.11	100.71	88.4
P5-255-13A 3	40.67	11.50	0.16	48.10	0.21	0.34	0.10	101.07	88.2
P5-255-13A 4	40.49	11.51	0.13	47.95	0.21	0.42	0.09	100.81	88.2
P5-255-13A 5	39.99	15.33	0.20	44.79	0.26	0.29	0.05	100.91	83.9
P5-255-13A 6	40.93	11.21	0.15	48.27	0.24	0.45	0.10	101.35	88.5
P5-255-13A 7	40.58	12.21	0.17	47.48	0.23	0.45	0.09	101.19	87.4
P5-255-13A 8	39.89	16.14	0.19	44.67	0.25	0.27	0.05	101.45	83.2
P5-255-13A 9	39.64	16.03	0.19	44.45	0.22	0.37	0.06	100.95	83.2
P5-255-13A 10	40.51	13.04	0.17	46.85	0.23	0.42	0.06	101.27	86.5
P5-255-13A 11	40.46	12.59	0.17	47.27	0.22	0.42	0.07	101.19	87.0
P5-255-13A 12	40.32	14.20	0.19	46.04	0.27	0.39	0.08	101.48	85.3
P5-255-13A 13	40.93	11.33	0.17	47.96	0.21	0.41	0.11	101.11	88.3
P5-255-13A 14	40.97	11.41	0.15	48.37	0.21	0.38	0.10	101.59	88.3
P5-255-13A 15	39.62	17.88	0.22	42.85	0.23	0.25	0.02	101.07	81.0
P5-255-9B 2	40.37	12.99	0.15	46.61	0.23	0.38	0.07	100.79	86.5
P5-255-9B 3	39.88	15.23	0.18	44.92	0.30	0.34	0.04	100.89	84.0
P5-255-9B 4	39.38	17.63	0.23	42.71	0.29	0.27	0.04	100.56	81.2
P5-255-9B 5	40.16	13.05	0.16	46.77	0.26	0.42	0.05	100.86	86.5
P5-255-9B 6	40.76	11.57	0.16	47.95	0.21	0.47	0.08	101.21	88.1
P5-255-9B 7	40.46	12.26	0.16	46.95	0.24	0.41	0.07	100.54	87.2
P5-255-9B 8	40.00	14.65	0.18	45.47	0.23	0.38	0.08	100.98	84.7
P5-255-9B 9	40.34	13.26	0.18	46.44	0.26	0.45	0.05	100.98	86.2
P5-255-9B 10	40.22	12.33	0.15	47.15	0.22	0.42	0.07	100.55	87.2
P5-255-9B 11	40.09	13.51	0.17	46.48	0.25	0.44	0.04	100.97	86.0
P5-255-9B 12	39.79	16.99	0.26	43.50	0.27	0.27	0.03	101.11	82.0
P5-255-9B 13	39.76	16.44	0.20	44.12	0.31	0.30	0.04	101.15	82.7
P5-255-9B 14	40.00	15.35	0.20	44.73	0.25	0.33	0.04	100.89	83.9
P5-255-9B 15	39.14	17.92	0.25	42.61	0.25	0.30	0.04	100.50	80.9
P5-255-3A 1	40.88	11.44	0.13	48.23	0.21	0.41	0.09	101.38	88.3
P5-255-3A 2	40.63	11.44	0.14	48.13	0.20	0.45	0.11	101.10	88.2
P5-255-3A 3	40.46	12.55	0.15	47.36	0.23	0.41	0.08	101.24	87.1
P5-255-3A 4	40.60	11.23	0.15	48.24	0.21	0.45	0.10	100.97	88.4
P5-255-3A 5	39.37	17.93	0.24	43.24	0.24	0.23	0.04	101.29	81.1
P5-255-3A 6	39.48	17.69	0.21	43.21	0.24	0.26	0.04	101.13	81.3
P5-255-3A 7	40.60	12.14	0.13	47.49	0.21	0.32	0.09	100.98	87.5
P5-255-3A 8	40.01	13.93	0.19	46.15	0.24	0.34	0.06	100.91	85.5
P5-255-3A 9	40.05	14.57	0.18	45.49	0.28	0.38	0.07	100.99	84.8
P5-255-3A 10	40.62	11.47	0.14	47.91	0.22	0.42	0.10	100.88	88.2
P5-255-16 1	40.50	12.50	0.15	47.03	0.22	0.33	0.07	100.80	87.0
P5-255-16 2	40.33	12.53	0.17	47.03	0.24	0.24	0.09	100.63	87.0
P5-255-16 3	40.37	12.54	0.19	46.87	0.23	0.31	0.07	100.59	87.0

P5-255-16 4	40.47	11.13	0.14	47.76	0.21	0.43	0.10	100.23	88.5
P5-255-16 5	40.11	13.32	0.17	46.24	0.27	0.24	0.08	100.44	86.1
P5-255-16 6	40.55	11.76	0.15	47.73	0.21	0.39	0.11	100.91	87.8
P5-255-16 7	40.44	12.05	0.14	47.36	0.20	0.38	0.09	100.67	87.5
P5-255-16 8	40.22	12.30	0.17	47.22	0.29	0.36	0.09	100.65	87.2
P5-255-16 9	40.35	12.76	0.17	46.78	0.24	0.32	0.06	100.67	86.7
P5-255-16 10	39.60	15.73	0.21	44.40	0.23	0.33	0.06	100.56	83.4
P5-255-16 11	40.06	14.55	0.22	45.68	0.24	0.36	0.05	101.15	84.8
P5-255-16 12	39.90	16.11	0.20	44.57	0.22	0.32	0.05	101.39	83.1
P5-255-16 13	40.67	11.22	0.14	48.12	0.21	0.39	0.09	100.84	88.4
P5-255-16 14	39.15	18.49	0.21	42.27	0.22	0.29	0.02	100.66	80.3
P5-255-16 15	39.31	17.15	0.19	43.42	0.23	0.33	0.02	100.65	81.9
P5-255-H 1	40.39	12.37	0.15	47.13	0.21	0.36	0.05	100.65	87.2
P5-255-H 2	40.14	13.34	0.17	46.08	0.21	0.38	0.10	100.42	86.0
P5-255-H 3	40.20	13.38	0.18	46.29	0.23	0.39	0.08	100.75	86.1
P5-255-H 4	39.27	17.90	0.20	42.97	0.23	0.29	0.04	100.90	81.1
P5-255-H 5	40.10	14.43	0.19	45.36	0.25	0.35	0.05	100.74	84.8
P5-255-H 6	39.95	14.48	0.19	45.54	0.26	0.38	0.05	100.85	84.9
P5-255-H 7	39.68	14.91	0.19	45.10	0.22	0.34	0.07	100.51	84.4
P5-255-H 8	39.27	17.98	0.23	42.66	0.23	0.23	0.04	100.64	80.9
P5-255-H 9	40.06	13.47	0.17	46.23	0.22	0.36	0.08	100.59	85.9
P5-255-H 10	40.53	11.53	0.14	47.82	0.20	0.42	0.10	100.73	88.1
P5-255-H 11	40.66	11.03	0.14	48.32	0.20	0.42	0.10	100.87	88.6
P5-255-H 12	39.78	15.39	0.23	44.74	0.26	0.30	0.04	100.74	83.8
P5-255-H 13	39.45	16.52	0.23	44.09	0.23	0.38	0.04	100.92	82.6
P5-255-H 14	40.14	14.02	0.17	45.77	0.26	0.43	0.05	100.83	85.3
P5-255-H 15	40.03	14.47	0.19	45.36	0.18	0.42	0.07	100.71	84.8
P5-255-B 1	39.36	15.10	0.19	45.45	0.28	0.27	0.08	100.73	84.3
P5-255-B 2	39.85	14.09	0.18	46.09	0.30	0.33	0.05	100.88	85.4
P5-255-B 4	40.63	11.89	0.15	47.85	0.22	0.44	0.10	101.26	87.8
P5-255-B 6	39.77	14.84	0.18	45.26	0.29	0.32	0.04	100.70	84.5
P5-255-B 7	38.96	19.05	0.26	41.71	0.29	0.25	0.02	100.55	79.6
P5-255-B 8	40.24	13.32	0.20	46.69	0.26	0.37	0.04	101.12	86.2
P5-255-B 9	39.40	15.55	0.20	44.99	0.25	0.38	0.04	100.80	83.7
P5-255-B 10	39.94	15.72	0.21	44.65	0.25	0.36	0.03	101.16	83.5
P5-255-B 11	40.07	13.15	0.17	46.84	0.26	0.29	0.07	100.85	86.4
P5-255-B 12	40.30	12.82	0.16	46.99	0.24	0.40	0.07	100.97	86.7
P5-255-B 13	39.23	18.98	0.25	41.93	0.29	0.30	0.04	101.03	79.7
P5-255-B 15	39.52	15.55	0.20	44.79	0.30	0.29	0.05	100.70	83.7
P5-255-14 1	39.37	16.13	0.22	44.28	0.24	0.33	0.05	100.61	83.1
P5-255-14 2	39.61	16.44	0.21	43.99	0.27	0.23	0.04	100.79	82.7
P5-255-14 3	39.48	16.41	0.19	44.12	0.26	0.22	0.03	100.71	82.7
P5-255-14 4	40.28	12.42	0.17	47.05	0.22	0.44	0.08	100.65	87.1
P5-255-14 5	38.78	20.59	0.25	40.58	0.23	0.30	0.02	100.75	77.8

P5-255-14 6	40.10	12.66	0.17	47.05	0.23	0.41	0.07	100.69	86.9
P5-255-14 7	40.38	12.65	0.15	46.99	0.23	0.36	0.08	100.83	86.9
P5-255-14 8	39.23	18.20	0.23	42.75	0.23	0.23	0.04	100.90	80.7
P5-255-14 9	40.71	11.67	0.19	47.89	0.22	0.39	0.08	101.15	88.0
P5-255-14 10	40.56	12.12	0.17	47.57	0.21	0.40	0.08	101.11	87.5
P5-255-14 11	40.29	12.26	0.16	47.13	0.23	0.37	0.08	100.51	87.3
P5-255-14 12	40.02	14.06	0.17	45.94	0.22	0.38	0.10	100.89	85.3
P5-255-14 13	40.09	14.55	0.20	45.65	0.23	0.36	0.06	101.15	84.8
P5-255-14 14	40.54	12.23	0.16	47.44	0.23	0.38	0.07	101.04	87.4
P5-255-14 15	40.12	13.99	0.15	46.07	0.26	0.32	0.06	100.97	85.4

1. Glass with S contents > 0.05 wt% (in bold) are submarine erupted, and the others are degassed and erupted subaerially (Dixon et al., 1991)

2. Standard Aoli olivine from a lherzolite xenolith from Kauai (White, 1966) yielded an average analysis of 40.63 % SiO_2, 49.46% MgO, 0.13% MnO, 0.38% NiO, 0.03% CaO, undetected Cr_2O_3, and 100.16% total compared with reported values of 40.5% SiO_2, 49.2% MgO, 0.13% MnO, 0.36% NiO, 0.02% CaO, and undetected Cr_2O_3. Synthetic Ni-olivine yielded an average analysis of 28.23% SiO_2, 70.95% NiO, <0.02% MgO, FeO, MnO, Cr_2O_3, and CaO, and a total of 99.24%.

3. Explanation of sample designations:
a - Glass labels such as P5-255-3-1, P5-255-3-4 etc are all from Duve location 3 (see Table 1) and the -1 and -4 identify multiple samples collected at location 3
b - Glass labels such as P5-255-12A-1, P5-255-12A-2 indicates different clasts in a scoop sample
c - Coexisting glass and olivine
d - MUD indicates glass grains in a short core
e - coexisting glass and olivine are indicated by identical labels in glass and olivine parts of the table; e.g., P5-255-13A-2

Table S3. Regression parameters for Penguin Bank Pb isotope array

	n	$^{207}Pb/^{206}Pb$ slope	2σ	χ^2_{red}	Age (Ga)	2σ	$^{208}Pb/^{206}Pb$ slope	2σ	χ^2_{red}	K	2σ
Penguin Bank	16	0.08155	0.0113	2.233	1.23	0.27	0.5250	0.0374	3.08	1.759	0.355

Regressions were performed using the Williamson [1968] method. Errors are reported at 95% confidence (2σ). χ2 red., reduced chi-squared.

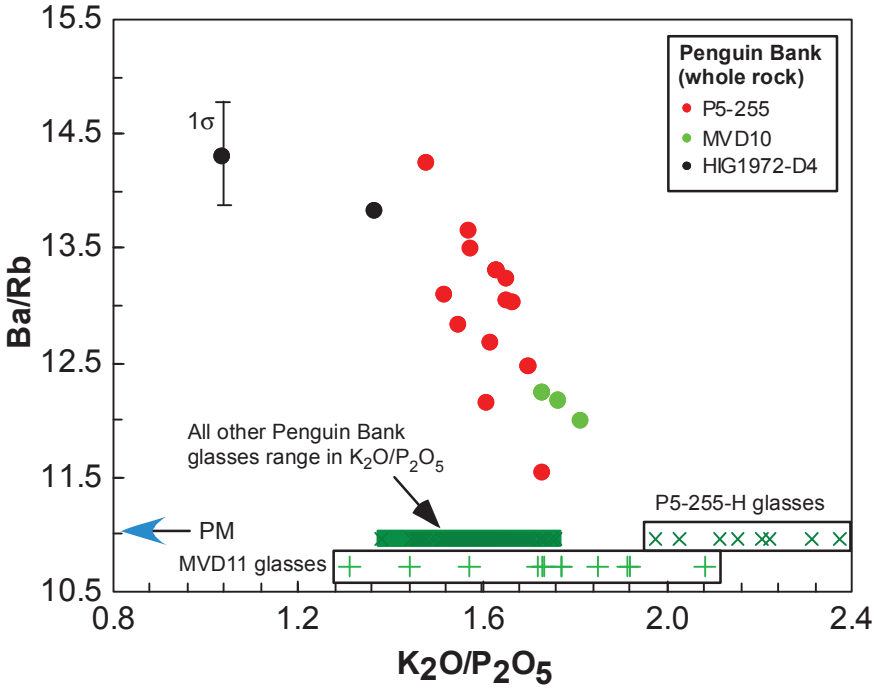

Fig. S1. Ba/Rb vs. K_2O/P_2O_5 – These ratios typically decrease and increase, respectively, during post-magmatic alteration of Hawaiian lavas (e.g., Feigenson et al., 1983). The Melville dredge (MVD10) and *Pisces V* dive (P5-255) samples have K_2O_5/P_2O_5 overlapping with the glass rinds (green rectangle); the P5-255-H glasses have anomalously high K_2O_5/P_2O_5 ratios. MVD11 glasses range from K_2O_5/P_2O_5 of 1.3 to 2.1. The HIG sample with the lowest K_2O/P_2O_5 and elevated Ba/Rb ratios may be more altered. The panel shows the 1σ uncertainty of 3% for Ba/Rb. PM denotes the value for primitive mantle from McDonough and Sun (1995).

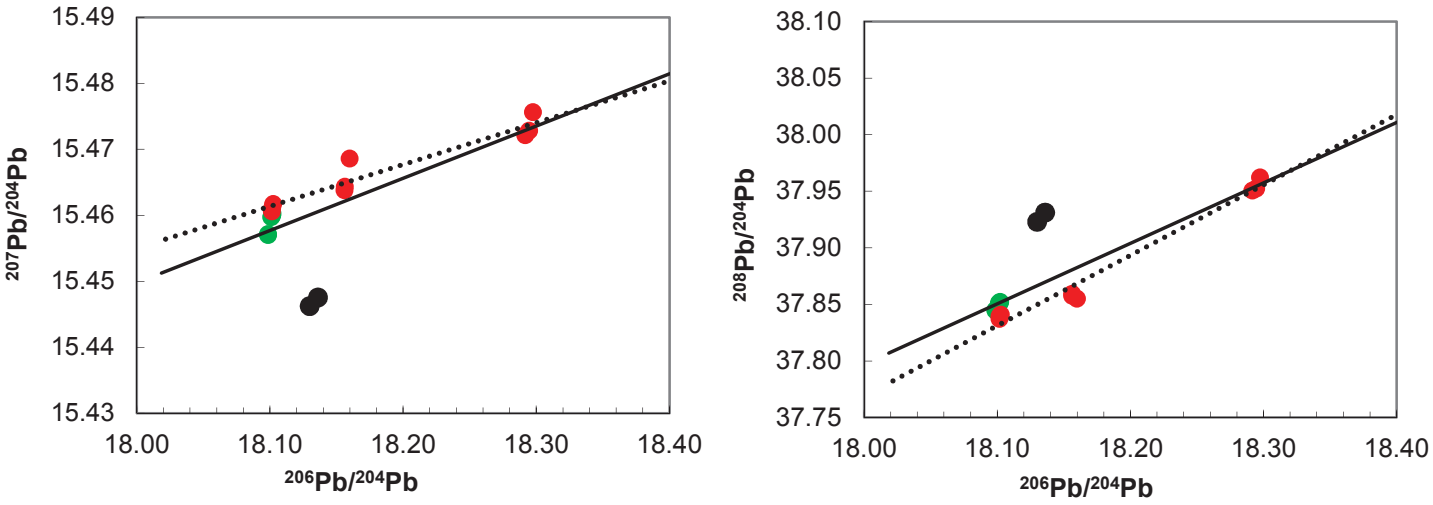

Fig. S2. Regression lines for Penguin Bank Pb isotope array. Solid line is for all Penguin Bank whole rock samples (n = 16) whereas dash line is for P5-255 samples only (n= 9).

Additional references

Dixon, J.E., Clague, D.A., Stolper, E.M., 1991. Degassing History of Water, Sulfur, and Carbon in Submarine Lavas from Kilauea Volcano, Hawaii. Journal of Geology 99: 371-394.

White, R., 1966. Ultramafic inclusions in basaltic rocks from Hawaii. Contributions to Mineralogy and Petrology 12: 245-314.

Williamson, J. H.,1968. Least-squares fitting of a straight line. *Can. J. Phys.* **46,** 1845–1847.